HHS Public Access

Author manuscript

Pharmacol Res. Author manuscript; available in PMC 2020 June 23.

Published in final edited form as:

Pharmacol Res. 2019 August ; 146: 104292. doi:10.1016/j.phrs.2019.104292.

Ablation of endothelial *Pfkfb3* protects mice from acute lung injury in LPS-induced endotoxemia

Lina Wang[1,2], **Yapeng Cao**[1,2], **B Gorshkov**[2], **Yaqi Zhou**[1], **Qiuhua Yang**[1,2], **Jiean Xu**[1,2], **Qian Ma**[1,2], **Xiaoyu Zhang**[1,2], **Jingjing Wang**[1], **Xiaoxiao Mao**[1], **Xianqiu Zeng**[1], **Yunchao Su**[3], **AD Verin**[2], **Mei Hong**[1], **Zhiping Liu**[1,2,*], **Yuqing Huo**[2,*]

[1]Drug Discovery Center, State Key Laboratory of Chemical Oncogenomics, Key Laboratory of Chemical Genomics, Peking University Shenzhen Graduate School, Shenzhen 518055, China

[2]Vascular Biology Center, Medical College of Georgia, Augusta University, Augusta, GA 30912, USA

[3]Department of Pharmacology and Toxicology, Medical College of Georgia, Augusta University, Augusta, GA 30912, USA

Abstract

Acute lung injury (ALI) is one of the leading causes of death in sepsis. Endothelial inflammation and dysfunction play a prominent role in development of ALI. Glycolysis is the predominant bioenergetic pathway for endothelial cells (ECs). However, the role of EC glycolysis in ALI of sepsis remains unclear. Here we show that both the expression and activity of PFKFB3, a key glycolytic activator, were markedly increased in lipopolysaccharide (LPS)-treated human pulmonary arterial ECs (HPAECs) *in vitro* and in lung ECs of mice challenged with LPS *in vivo*. *PFKFB3* knockdown significantly reduced LPS-enhanced glycolysis in HPAECs. Compared with LPS-challenged wild-type mice, endothelial-specific *Pfkfb3* knockout (*Pfkfb3*$^{\Delta VEC}$) mice exhibited reduced endothelium permeability, lower pulmonary edema, and higher survival rate. This was accompanied by decreased expression of intracellular adhesion molecule-1 (Icam-1) and vascular cell adhesion molecule 1 (Vcam-1), as well as decreased neutrophil and macrophage infiltration to the lung. Consistently, *PFKFB3* silencing or PFKFB3 inhibition in HPAECs significantly downregulated LPS-induced expression of ICAM-1 and VCAM-1, and monocyte adhesion to HPAECs. In contrast, adenovirus-mediated *PFKFB3* overexpression upregulated ICAM-1 and VCAM-1 expression in HPAECs. Mechanistically, *PFKFB3* silencing suppressed LPS-induced nuclear translocation of nuclear factor κB (NF-κB)-p65, and NF-κB inhibitors

Address correspondence to: Yuqing Huo, MD, PhD, Vascular Biology Center, Department of Cellular Biology and Anatomy, Medical College of Georgia, Augusta University, Phone: 706-721-4414 (Office), Fax: 706-721-9799 (VBC), yhuo@augusta.edu.

*equally contributed to the work.

Author contributions

LW, MH, ZL and YH designed the research; LW, YC, GB, ZL, YZ, QY, JX, QM, XZ, JW, XM and XZ performed experiments; LW, GB, ZL and YH analyzed data; LW, ZL and YH wrote and revised the manuscript; ZL, VAD, MH and YH provided reagents or materials and participated in experimental design.

Conflict of Interest Statement

The authors declare no conflicts of interest.

Ethics statement

This study was carried out in strict accordance with the recommendations of Committee on the Use of Human and Animal Subjects of Augusta University. The protocols were approved by the IACUC at Augusta Universtiy.

abrogated PFKFB3-induced expression of ICAM-1 and VCAM-1. Finally, administration of the PFKFB3 inhibitor 3PO also reduced the inflammatory response of vascular endothelium and protected mice from LPS-induced ALI. Overall, these findings suggest that targeting PFKFB3-mediated EC glycolysis is an efficient therapeutic strategy for ALI in sepsis.

Graphical Abstract

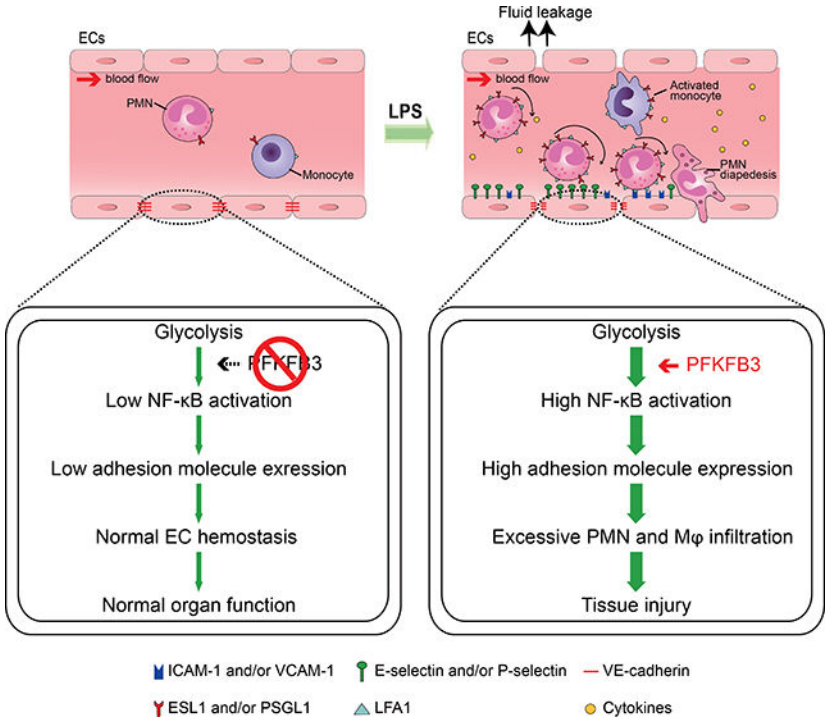

Keywords

Sepsis; Endothelial cell; PFKFB3; Glycolysis; Inflammation

1. Introduction

Sepsis is a clinical syndrome invoked by infection or injury with a detrimental impact on microvascular metabolic and immune-inflammatory homeostasis (1–3). Excessive inflammatory responses, which can cause severe cell and tissue damage and organ dysfunction such as acute lung injury (ALI), are the important pathological features of sepsis (4–8). Endothelial cells (ECs) located on the inner wall of blood vessels mediate vascular tone as well as the balance of pro-inflammatory and anti-inflammatory responses (9). Endothelial activation and dysfunction evidenced by upregulation of adhesion molecules and increased leukocyte adhesion are hallmarks of sepsis, which can induce multiple-organ dysfunction (10). EC metabolism has been linked to EC function and vascular physiology and pathology (11, 12). However, the role of EC metabolism in organ injury in sepsis, especially in ALI, remains unclear.

Aberrant metabolism, particularly increased aerobic glycolysis or the Warburg effect, has been involved in the pathogenesis of sepsis (13). Most patients with sepsis and septic shock show an increased concentration of lactate, the end-product of aerobic glycolysis, in blood serum (14). Clinically, the plasma lactate level and lactate clearance rate are diagnostic indicators that correlate with illness severity and mortality (15–17). The energy production and macromolecule synthesis in ECs is mainly dependent on glycolysis (11), which is a metabolic biological process that converts glucose to pyruvate and lactate. 6-phosphofructo-1-kinase (PFK1) is the second rate-limiting enzyme of the glycolysis pathway and can be activated by fructose-2,6-bisphophate (F-2,6-P2) (18, 19). As a potent allosteric activator, F-2,6-P2 is mainly regulated by PFK-2/FBPase (PFKFB) family (20). Of all PFKFB isoenzymes, PFKFB3 is the most abundant isoenzyme in various EC subtypes and exerts the highest kinase to bisphosphatase activity (740:1) to sustain a high glycolytic rate (11, 21). It has been reported that endothelial PFKFB3-driven glycolysis regulates tumor growth (22), vessel sprouting (11) and pathological angiogenesis (23, 24); however, the role of endothelial PFKFB3 in ALI and sepsis has not yet been clearly studied.

In this study, both genetic and pharmacological approaches were used to investigate the consequence of endothelial *Pfkfb3* depletion or inhibition on endothelial inflammatory responses, endothelial barrier dysfunction, lung edema, cardiac function, kidney injury and survival outcome in a widely used lipopolysaccharide (LPS)-induced murine sepsis model. Our observations suggest that endothelial-specific *Pfkfb3* deficiency or PFKFB3 inhibitor 3-(3pyridinyl)-1-(4-pyridinyl)-2-propen-1-one (3PO) dramatically alleviates lung edema and improves survival outcome in the LPS-induced murine sepsis model, which is highly dependent on the reduction of leukocyte infiltration and endothelial permeability. Mechanistically, *Pkfbf3* deletion or inhibition decreases leukocyte recruitment by inhibiting adhesion molecule expression via inactivation of nuclear factor κB (NF κB) signaling in ECs. To the best of our knowledge, these findings uncover, for the first time, a critical role of endothelial PFKFB3 in ALI of sepsis *in vivo*, and our results indicate that PFKFB3 can be a potential target for ALI therapy.

2. Methods and materials

2.1. Animals

Animals were maintained at Augusta University, and the protocol was approved by the IACUC at Augusta Universtiy. The floxed *Pfkfb3* (*Pfkfb3*$^{lox/lox}$) mice were generated by Xenogen Biosciences Corporation (Cranbury, NJ, USA) (24). Conditional endothelial *Pfkfb3* deficient mice (*Pfkfb3*$^{lox/lox}$ *Cdh5*^{Cre}) were generated by breeding *Pfkfb3*$^{lox/lox}$ mice with *Cdh5*^{cre} transgenic mice (Stk. No. 006137, The Jackson Laboratory, Bar Harbor, ME, USA). All mice were on a C57BL/6J background. Age-, sex- and body weight-matched, 8-to12-week-old *Pfkfb3*^{WT} and *Pfkfb3*$^{\Delta VEC}$ mice were used in the study. For 3PO treatment, wild-type (WT) C57/BL6 mice were administered 3PO at a dose of 50 mg/kg for 3 hours before LPS challenge. For the survival study, LPS (Sigma-Aldrich, St. Louis, MO, USA) or vehicle was administered at 12.5 mg/kg body weight by i.p. injection to induce sepsis. The mice had normal access to food and water and were monitored twice a day over the course of 10 days.

2.2. Materials

LPS (0127:B8) and dimethyl sulfoxide (DMSO) were purchased from Sigma-Aldrich (Louis, MO, USA). Collagen type II (Cat. No. NC9693955) was from Fisher Scientific (Pittsburgh, PA, USA). 3PO was from Merck Millipore (Burlington, MA, USA). BAY 11–7085 (Cat. No. BML-EI279) and Pyrrolidinedithiocarbamic acid (PDTC) (Cat. No. ALX-400–002) were from Enzo Life Sciences (New York, NY, USA).

2.3. Vascular permeability assessment

Vascular permeability was detected as described previously (25). Briefly, LPS (1 mg/kg body weight) or 0.9% saline was intratracheally (i.t.) injected via a 20-gauge catheter. In order to assess vascular leak, Evans blue dye (EBD) was injected into the tail vein 120 minutes before tissue collection. Bronchoalveolar lavage (BAL) was centrifuged at 1500 g for 15 min and the subsequent supernatant was used for measurement of total protein using the BCA protein assay kit (Cat. No. 23225, Pierce/Thermo Fisher Scientific, Grand Island, NY, USA). Then the lungs were perfused with PBS and collected for EBD analysis. EBD was extracted in formamide at 60°C for 18 hours, the supernatants were measured at 620 nm spectrophotometrically.

2.4. Echocardiography

Echocardiograms were performed at baseline, 6 hours and 24 hours after LPS injection. Two-dimensional echocardiography was performed using a Visual Sonics Vevo 2100 ultrasound machine with a 40 MHz ultrasound probe (MS-400). Briefly, mice were anesthetized with continuous isoflurane inhalation (1.0–3.0%) and placed on a heated pad in a supine position. The percentage of left ventricular (LV) fractional shortening (FS%) and ejection fraction (EF%), LV stroke volume (μl), cardiac output (ml/min), and LV end-systolic and diastolic diameter were obtained from the parasternal short axis view using M-mode.

2.5. Histology

The mouse lungs and kidneys were flushed with phosphate buffered saline (PBS) and perfused with 4% paraformaldehyde (PFA). Fixed tissues were embedded into paraffin block and sectioned at 5 μm thickness. Hematoxylin and eosin (H & E) staining was performed to show lung edema and kidney injury. For kidney injury score, 10 randomly and non-overlapping fields were chosen for each animal. Scoring reflected the grading of tubular necrosis, loss of brush border, cast formation, vacuolization and tubule dilation as follows: 0 (none), 1 (<25%), 2 (25–50%), 3 (50–75%) and 4 (75–100%)(26).

2.6. Immunostaining analysis

For Pfkfb3, Icam-1, Vcam-1 and VE-cadherin immunostaining, deparaffinized and dehydrated lung sections were boiled at 98°C for 10 min for antigen retrieval followed by blocking with 10% normal goat serum for 1 h at room temperature. Sections were incubated with anti-CD31 (1:200, Cat. No. DIA-310, Dianova, Hamburg, Germany), anti-PFKFB3 (1:200, Cat. No. ab181861, abcam, Cambridge, MA, USA), anti-ICAM-1(1:200, Cat. No. sc-8439, Santa Cruz Biotechnology, Dallas, TX, USA), anti-VCAM-1(1:200, Cat. No.

ab134047, abcam) or anti-VE-cadherin (1:200, Cat. No. PAF-19612, Invitrogen/Thermo Fisher Scientific) at 4°C overnight. For cellular VE-cadherin immunostaining, HPMVECs were grown on 8-well culture slides (Corning). After treatment, HPMVECs were fixed with 4 % PFA for 20 minutes at room temperature, incubated with 0.25% Triton X-100 to permeabilize the cells, blocked with 10% normal goat serum, and incubated with anti-VE-cadherin (1:200, Cat. No. MAB 9381, R&D, Minneapolis, MN, USA) at 4°C overnight. Then the sections and slides were incubated with AlexaFluor conjugated isotype-specific secondary antibodies (1:250, Invitrogen, Grand Island, NY, USA) for 1 h at room temperature. The nuclei were stained with DAPI (1 μg/mL, Thermo Fisher Scientific) for 5 minutes at room temperature, and the samples were mounted with mounting media (Cat. No. H-1000, Vector Laboratories, Burlingame, CA, USA). The sections were imaged with a confocal microscope (LSM780; Carl Zeiss, Göttingen, Germany).

For intracellular adhesion molecule-1 (ICAM-1), vascular cell adhesion molecule 1 (VCAM-1), Mac2 and Ly6G immunohistochemical (IHC) staining on mouse lungs, 5 μm sections were first deparaffinized and dehydrated. Endogenous peroxidase activity was destroyed with H_2O_2 (3 ml 30% H_2O_2 in 200 ml methanol) for 30 min at room temperature. The sections were then boiled in 10 mmol/L sodium citrate (pH 6.0) at 98 °C for 10 min for antigen retrieval. After blocking with avidin solution with 10% normal rabbit serum for 1h, sections were incubated with primary antibodies in biotin blocking solution against anti-ICAM-1 (3 μg/ml, ab25375, Abcam, Cambridge, MA, USA), anti-VCAM-1 (3 μg/ml, 1510–01, Southern Biotech, Birmingham, AL, USA), anti-Mac2 (3 μg/ml, ACL8942F, Accurate Chemical & Scientific Corporation, Westbury, NY, USA), or anti-Ly6G (3 μg /ml, 551459, BD biosciences, San Jose, CA, USA) antibodies at 4°C overnight. Lung sections were incubated with a biotinylated rabbit anti-rat IgG (H+L) secondary antibody (1:200, Cat. No.BA-4001, Vector Laboratories) for 1 hour, followed by incubation with ABC solution (Cat. No.PK-6100, Vector Laboratories) for 30 min at room temperature. Peroxidase substrate 3, 3’-diaminobenzidine (Cat. No.3468, Dako, Santa Clara, CA, USA) was used to detect the antibodies according to the manufacturer’s instructions. The sections were counterstained with hematoxylin I (Cat. No. GHS116, Sigma) for 30s at room temperature, then dehydrated and mounted with xylene-based mounting medium (Cat. No. 8312–4, Richard-Allan Scientific, San Diego, CA, USA). Quantification of Mac2 and Ly6G staining was performed using the Image-J software. Data were reported as a mean of positive staining cell number on eight sections per lung.

2.7. Flow cytometry

The lungs were perfused with PBS and digested with collagenase II (Worthington, 2 mg/ml in serum-free DMEM, Corning, NY, USA), followed by mincing with a 20-gauge needle seven times. The cells were then pelleted at 500 g for 5 min at 4 °C, lysed with red blood cell lysis buffer (Cat. No. R7767, Sigma-Aldrich), washed and filtered through a 70 μm nylon filter, and resuspended in FACS buffer. Prior to staining, Fc-γR was blocked with anti-CD16/32 Ab (Cat. No. 553142, BD Biosciences) for 15 min. Cells were stained for 30 min on ice with a combination of the following Abs: CD45-PerCP (Cat. No. 561869, BD Biosciences), F4/80-PE (Cat. No. 565410, BD Biosciences), CD11b-FITC (Cat. No. 11–0112-85, eBioscience, San Diego, CA, USA), CD45-APC (Cat. No. 558702, BD

Biosciences), CD11b-PerCP (Cat. No. 550993, BD Biosciences) and Ly6G-FITC (Cat. No. 551460, BD Biosciences). Prior to flow cytometry, cells were washed, pelleted and resuspended in FACS buffer. Flow cytometry analysis was conducted at the Augusta University Flow Cytometry Center using a BD FACSCalibur (BD Pharmingen, San Jose, CA, USA), and the data were analyzed using FlowJo software.

2.8. Mouse lung EC isolation

ECs in mouse tissues were isolated using CD31-microbeads as described previously (27). Briefly, mouse lungs were minced and digested with collagenase II (Worthington, 2 mg/ml in serum-free DMEM, Corning) for 30 min at 37 °C, resuspended into a single-cell suspension followed by filtering through a 70-μm cell strainer (Corning), and centrifuged at 400 g for 5 min at 4 °C to pellet cells. The cells were resuspended in 100 μL pre-cooled PBS with 0.5% BSA and 2 mM EDTA, and incubated with CD31-microbeads (Miltenyi Biotec, Bergisch Gladbach, Germany) for 15 min on ice. After affinity binding, the CD31-positive cells were collected with a MACS separator (Miltenyi Biotec) according to the manufacturer's instructions.

2.9. Cell culture and treatment

Human pulmonary artery endothelial cells (HPAECs, Cat. No. CC-2530, Lonza, NJ, USA) and human pulmonary microvascular endothelial cells (HPMVECs, Cat. No. CC-2527, Lonza, NJ, USA) were cultured in Vessel Cell Basal Medium (VCBM, ATCC, Manassas, VA, USA) supplemented with Microvascular Endothelial Cell Growth Kit-BBE (ATCC) and 1% penicillin/streptomycin (Cat. No. 15–140-122, Fisher Scientific). HPAECs and HPMVECs between passages 3 to 8 were used in experiments. For LPS treatment, the culture medium was changed to 25% VCBM (25% VCBM complete medium + 75% VCBM basal medium) and cultured for 12 hours followed by 1 μg/ml LPS treatment for the indicated time. For 3PO treatment, HPAECs were pretreated with vehicle or 20 μM of 3PO for 30 min followed by exposure to 1 μg/ml LPS for 4 hours.

Human monocytic THP-1 cells (ATCC) were maintained in RPMI 1640 medium supplemented with 10% heat-inactivated FBS, 2 mM L-glutamine and 1% penicillin/streptomycin as described previously (28). Mouse lung endothelial cells (MLECs) were isolated using CD31 microbeads as described above, and purified ECs were plated on matrigel-coated 6-well plates and lysed for analysis after growing 5 to 7 days in Endothelial Cell Growth Medium-2 (EGM-2) complete media.

2.10. Metabolic assay

Real-time changes in extracellular acidification rate (ECAR) of HPAECs were analyzed with an XF96 Extracellular Flux Analyzer (Seahorse Bioscience, North Billerica, MA, USA) as described previously (27). Briefly, HPAECs were seeded at 2.5×10^4 per well on Seahorse XF96 polystyrene tissue culture plates (Seahorse Bioscience) and incubated at 37 °C overnight in VCBM. The next day, after 1 μg/ml LPS treatment for 4 hours, the medium was changed to XF base Medium (Seahorse Bioscience) supplemented with 2 mM glutamine, and then the plate was incubated for 1 h in a non-CO_2 incubator at 37 °C. The ECAR assay was performed on the XF96 extracellular flux analyzer (Seahorse Bioscience), and the

ECAR values were normalized using protein concentration. Inhibitors and activators were used in these tests at the following concentrations: glucose (10 mM), oligomycin (2 μM), 2-DG (50 mM).

2.11. F-2,6-P2 level assay

F-2,6-P2 was detected with the previously described method (29). HPAECs were homogenized with 0.05 M NaOH, and heated for 5 min at 80°C. After cooling, the samples were centrifuged and the supernatants were neutralized with acetic acid. The mixture was centrifuged and the levels of F-2,6-P2 in the supernatant were measured by the stimulation of PPi-PFK assayed in the presence of 0.5 mM pyrophosphate and 1 mM fructose 6-phosphate in the assay mixture as shown in the table below. Measurement was conducted at 340nm with Synergy H1 Hybrid Reader (BioTek, Winooski, Vermont, USA) The values were normalized using protein concentration.

2.12. Lactate assay

The lactate levels of the HPAECs were measured with the Lactate Assay Kit (Cat. No. MAK064, Sigma) according to the manufacturer's instructions.

2.13. Adenovirus transduction of HPAECs

HPAECs grown at 70% – 80% confluence were incubated with 500 μL basal medium containing Ad-*CTRL* or Ad-*PFKFB3* adenovirus that carries an epitope tag containing both Flag and His motifs (Cat, No. VH840078, Vigene Biosceiences, Rockville, MD, USA). After 2 hours, the medium was replaced with fresh complete VCBM followed by continuous culture for 48 hours. The cells were then treated as indicated and collected for Western blot and real-time PCR analyses.

2.14. Monocyte adhesion assay

Monocyte adhesion assay was performed according to protocols as described previously with some modifications (30, 31). Briefly, the THP-1 cells labeled with Calcein-AM (Cat. No. 354216, Corning, New York, USA) were incubated with the confluent monolayer of HPAECs or HPMVECs pretreated with LPS for 4 hours. 30 min after incubation, non-adherent cells were removed by washing three times with RPMI 1640 media followed by fixing with 4% PFA. Images were taken under the fluorescence microscope. Fluorescent-positive cells were counted with Image J and normalized with total cell numbers of HPAECs or HPMVECs.

2.15. Small interfering RNA (siRNA) interference of HPAECs

When HPAECs and HPMVECs were grown to 80% confluence, the cells were transfected with 25 nM of siRNAs targeting human *PFKFB3* (si*PFKFB3*, Cat. No. L-006763–00-0005; Dharmacon, Lafayette, CO, USA) or non-targeting negative control (si*CTRL*, Cat. No.L-004018–00-0005; Dharmacon) using Lipofectamine RNAi Max reagent (Cat. No 13778–150; Invitrogen) according to the manufacturer's protocol. Six hours later, the medium was changed to fresh complete VCBM for continuous culture. Forty-eight hours

after siRNA transfection, the cells underwent different treatments and were then collected for various assays.

2.16. Western blot

Cells or lung samples were lysed with RIPA buffer containing protease inhibitor cocktails (Cat. No. 05892970001, Roche, Indiana, IN, USA) as described previously (27). After sonication and centrifugation of cell lysates, protein concentration was measured with the BCA assay and then 20 μg of protein was loaded onto the 7.5%−10% sodium dodecyl sulfate polyacrylamide gel electrophoresis (SDS-PAGE) gel. Following electrophoresis, blotting, and blocking in 5% skim milk, blots were probed with the following primary antibodies: PFKFB3 (1:1000, Cat. No. ab181861, abcam), ICAM-1 (1:1000, Cat. No. sc-8314, Santa Cruz Biotechnology for human; 1:1000, Cat. No. ab25375, Abcam for mice), VCAM-1 (1:1000, Cat. No. 13662, CST, Danvers, MA, USA), p65 (1:1000, Cat. No. 8242, CST), and p-p65 (1:1000, Cat. No. 3033, CST). Anti-β-actin (1:1000, Cat. No. sc47776, Santa Cruz Biotechnology) was used as loading control.

2.17. RNA isolation and quantitative real-time PCR

The total RNA from HPAECs or mouse lung samples were extracted using Trizol reagent (Cat. No. 15596018; Invitrogen). 0.5–1μg of RNA was used as a template for reverse transcription with iScript cDNA synthesis kit (Cat. No. 170–8891; Bio Rad, Hercules, California, USA). qPCR was performed with universal SYBR green mix (Cat. No. 172–5122, BioRad) on the StepOne Plus System (Applied Biosystems, Grand Island, NY). PCR amplification consisted of 10 min of an initial denaturation step at 95 °C, followed by 40 cycles of PCR at 95 °C for 15 s, and 60 °C for 1 min. Relative gene expression was converted using the $2^{-\Delta\Delta CT}$ method against the internal control 18s RNA, and data were presented as fold change relative to control groups.

2.18. Statistical analysis

Statistical information is indicated in the figure legends. The significance of the differences between two groups was assayed using unpaired Student's *t* test. Multiple comparisons were performed by one-way ANOVA followed by Bonferroni's *post hoc* test. Statistical analysis was performed with GraphPad Prism (LaJolla, CA, USA). Kaplan Meier survival curves were compared using log-rank Mantel-Cox test. All results are presented as mean ± SEM. $p < 0.05$ was considered significant (* $p < 0.05$, ** $p < 0.01$, *** $p < 0.001$).

3. Results

3.1. Expression and activity of PFKFB3 are increased in the in vivo and in vitro models of LPS-induced ALI

Emerging evidence suggests the involvement of cellular metabolism in the pathogenesis of ALI (32–34). It has been shown that glycolysis in lung is elevated in patients with ALI (35–37), although the mechanisms underlying this remain unclear. To determine whether the glycolytic activator PFKFB3 is responsible for the increased glycolysis, we analyzed Pfkfb3 expression in the lungs of mice that had ALI induced by i.p. injection of 12.5 mg/kg body weight LPS for 6 hours. Strikingly, both the mRNA and protein levels of Pfkfb3 were

significantly increased in the lungs of mice challenged with LPS compared with that of control mice (Fig.1A and 1B).

The lung endothelium is a major metabolic tissue that is critically involved in the pathogenesis of ALI (38). CD31 is a membrane glycoprotein which is highly expressed on endothelial cells, we isolated lung ECs using CD31 microbeads and compared Pfkfb3 expression in the whole cell lysate, CD31-positive and CD31-negative cells of the lung. Western blotting showed that the protein level of Pfkfb3 was markedly increased in the whole cell lysate of the lung and CD31-positive cells, and only modestly increased in CD31-negative cells, indicating that CD31 positive cells were the major cellular origin for the upregulated Pfkfb3 in the lungs of LPS-treated mice (Fig.1C). As CD31 also expressed on platelets and leukocytes, to further determine whether increased Pfkfb3 expression is mainly attributed to ECs in LPS-treated lungs, we did double immunofluorescence staining of lung sections using a well-characterized monoclonal antibody for Pfkfb3 (39, 40) and the EC marker CD31, the results showed that Pfkfb3 expression on the endothelial layer of pulmonary arteries was markedly increased compared with that on the endothelial layer of control mice (Fig.1D).

To further confirm whether LPS was able to stimulate PFKFB3 expression in ECs *in vitro*, MLECs and HPAECs were treated with 1 μg/ml LPS for up to 18 hours. Indeed, PFKFB3 protein levels were increased following LPS treatment in both cell types (Fig. 2A and 2B). Moreover, we noticed a marked increase in PFKFB3 activity, as evidenced by an increased level of Fructose 2,6-bisphosphate (F-2,6-P2) in LPS-treated HPAECs (Fig. 2C). Since PFKFB3 is a potent glycolytic activator, we further assessed the glycolytic function of LPS-treated HPAECs transfected with si*CTRL* or si*PFKFB3* using both lactate measurement and Seahorse Flux analysis. As shown in Fig. 2D, LPS treatment markedly increased the PFKFB3 protein level, while about 75% of PFKFB3 protein expression was depleted after transfection with si*PFKFB3* for 48 h. LPS treatment significantly elevated lactate production and glucose-induced glycolysis and also increased the maximal glycolytic capacity, which were completely abrogated by *PFKFB3* deletion in HPAECs (Fig. 2E–J). Altogether, these results indicate that high levels of expression and activity of EC PFKFB3 contribute to the increased glycolysis in ALI.

3.2. Endothelial-specific Pfkfb3 deficiency protects mice from LPS-induced ALI and sepsis

To gain insight into whether endothelial Pfkfb3 plays a causal role in the LPS-induced ALI model in mice, we used endothelial-specific *Pfkfb3*-deficient mice generated by breeding *Pfkfb3*$^{lox/lox}$ mice with *Cdh5*^{cre} transgenic mice (24) (Fig. 3A). Western blot analysis showed that Pfkfb3 amounts were dramatically decreased in MLECs from *Pfkfb3*$^{\Delta VEC}$ mice compared with those from *Pfkfb3*^{WT} mice, thus confirming the effective endothelial *Pfkfb3* deletion in *Pfkfb3*$^{\Delta VEC}$ mice (Fig. 3B). To further verify the endothelium-specific *Pfkfb3* deletion in *Pfkfb3*$^{\Delta VEC}$ mice, double immunofluorescence staining was used to detect EC Pfkfb3 expression in the pulmonary endothelium. We found no noticeable changes in the expression of Pfkfb3 in smooth muscle cells (SMCs) or other non-ECs, whereas expression

of Pfkfb3 was markedly decreased in ECs of *Pfkfb3*$^{\Delta VEC}$ mice compared with those of *Pfkfb3*^{WT} mice (Fig. 3C).

To examine the biological consequence of endothelial Pfkfb3 in LPS-induced sepsis, *Pfkfb3*$^{\Delta VEC}$ and *Pfkfb3*^{WT} mice were challenged with a lethal dose (12.5 mg/kg) of LPS by i.p. injection. Animal mortality was monitored following LPS injection. As shown in Fig. 4A, all the *Pfkfb3*^{WT} mice had died by 5 days (120 hours) post-LPS challenge whereas only 55% of *Pfkfb3*$^{\Delta VEC}$ mice died in the same period, indicating that endothelial Pfkfb3 upregulation by LPS treatment contributes to LPS-induced death. Accordingly, the cardiac dysfunction (Fig. 4B–4G) and kidney injury (Fig. S1) were also decreased in *Pfkfb3*$^{\Delta VEC}$ mice compared with those of *Pfkfb3*^{WT} mice. Disruption of the endothelial barrier integrity and consequent pulmonary edema are typical symptoms of ALI (41). To determine the *in vivo* consequences of loss of endothelial Pfkfb3 on ALI and endothelial barrier function, we next determined alterations in vascular permeability by H&E staining and Evans blue dye (EBD) assay. *Pfkfb3*$^{\Delta VEC}$ and *Pfkfb3*^{WT} mice were injected with either sterile saline or LPS by i.t. injection for 6 hours. The H&E staining showed that *Pfkfb3*$^{\Delta VEC}$ mice had a lower degree of lung edema (Fig. 5A). The protein levels in the BAL and EBD in lung tissue were significantly decreased in *Pfkfb3*$^{\Delta VEC}$ mice compared with those of *Pfkfb3*^{WT} mice after LPS challenge, indicating that LPS-induced endothelium hyper-permeability was blunted in *Pfkfb3*$^{\Delta VEC}$ mice (Fig. 5B and 5C). The lung wet-to-dry (W/D) ratio, which was used as an index to evaluate lung edema, was lower in LPS-injured *Pfkfb3*$^{\Delta VEC}$ lungs compared with the LPS-injured *Pfkfb3*^{WT} lungs (Fig. 5D). Since microvascular barrier function depends on the junction proteins at the endothelial cell-cell borders, we further evaluated the VE-cadherin expression in ECs by immunofluorescence staining of lung sections. The results showed that upon LPS treatment, the expression of VE-cadherin in the ECs of lungs of *Pfkfb3*$^{\Delta WT}$ mice was lower than that in *Pfkfb3*$^{\Delta VEC}$ mice compared with that of control mice (Fig. 5E). We also detected the expression of VE-cadherin in the HPMVECs transfected with si*CTRL* or si*PFKFB3* with the treatment of 1μg/ml LPS for 4 hours. The results showed that VE-cadherin expressed in the AJ of HPMVEC monolayer, and upon treatment with LPS, VE-cadherin appear to be dissociated from AJ and si*PFKFB3* was able to suppress these effects (Fig. S2).

Overall, these findings suggest that endothelial *Pfkfb3* deficiency protects mice from LPS-induced ALI and death, and is accompanied by improved cardiac and kidney function.

3.3. Endothelial Pfkfb3 is required for leukocyte recruitment and endothelial inflammation in vivo.

Neutrophil and macrophage recruitment and activation, pivotal processes of ALI (42–45), are highly dependent on the expression of adhesion molecules on vascular ECs (10). We therefore asked whether *Pfkfb3* deficiency rendered ECs less adhesiveness for neutrophils and macrophages via decreased adhesion molecule expression. We first analyzed the effects of LPS on neutrophil and macrophage infiltration by performing flow cytometry analyses of lungs from *Pfkfb3*^{WT} and *Pfkfb3*$^{\Delta VEC}$ mice exposed to 12.5 mg/kg LPS for 6 hours. Using Ly6G and CD11b as neutrophil markers and F4/80 and CD11b as interstitial macrophage markers respectively, we examined the numbers of neutrophils and macrophages in the lungs

by flow cytometry. We found that LPS significantly increased the number of neutrophils and macrophages in lung, which were blunted by endothelial *Pfkfb3* deficiency (Fig. 6B and 6D). Using Ly6G as a neutrophil marker and Mac2 as a macrophage marker, we further examined the infiltrated neutrophils and macrophages in lung sections by immunostaining. Consistently, the numbers of infiltrated neutrophils and macrophages were decreased in *Pfkfb3*$^{\Delta VEC}$ mice 6 hours after LPS challenge compared with those of *Pfkfb3*^{WT} mice (Fig. 6A and 6C). These results suggest that endothelial *Pfkfb3* deficiency impaired neutrophil and macrophage recruitment to the lungs in response to LPS challenge.

Given that the recruitment of macrophages and neutrophils is mainly dependent on the expression of cytokines and adhesion molecules, especially Icam-1 and Vcam-1 (46), we next analyzed the effects of Pfkfb3 deficiency on cytokine production and adhesion molecule expression in lung ECs *in vivo* by qPCR, Western blot, DAB immunostaining and immunofluorescence staining. *Pfkfb3*^{WT} and *Pfkfb3*$^{\Delta VEC}$ mice were challenged with 12.5 mg/kg LPS for 6 hours, and MLECs were isolated for qPCR analysis. The results showed that the mRNA levels of *Icam-1*, *Il-1β*, *Tnf-α*, *Cxcl-10* and *E-selectin* were decreased in *Pfkfb3*$^{\Delta VEC}$ mice compared with those of control mice upon LPS treatment (Fig. 7A–7E). Western blot analysis revealed that LPS markedly induced the expression of Icam-1 in the lungs of *Pfkfb3*^{WT} mice but not that of *Pfkfb3*$^{\Delta VEC}$ mice, and this was also true for Icam-1 expression of isolated MLECs from these mice (Fig. 7F–7G). Icam-1 and Vcam-1 staining on the lung sections also showed that the expression of Icam-1 and Vcam-1 on ECs were attenuated in *Pfkfb3*$^{\Delta VEC}$ mice (Fig. 7H–7K). Thus, *Pfkfb3* deficiency in ECs is able to prevent LPS-induced expression of Icam-1 and Vcam-1 in lung.

3.4. PFKFB3 inhibitor 3PO protects mice from LPS-induced ALI by inhibiting endothelial inflammation

To further examine the role of PFKFB3 on ALI and sepsis, we examined the effects of pharmacological inhibition of PFKFB3. To this end, 3PO, a specific PFKFB3 inhibitor, was administered to the wild-type mice 3 hours before LPS challenge at a dose of 50 mg/kg (21), followed by the treatment with 12.5 mg/kg LPS by i.p. injection. The animal survival rate was obtained after LPS injection. We found that 3PO treatment showed a beneficial effect on the survival outcome in the LPS-induced sepsis model. As shown in Fig. 8A, all the mice treated with vehicle died within 4 days, while only 60% of mice with 3PO treatment died within the same period. H&E staining revealed that 3PO-treated mice exhibited decreased edema and leukocyte infiltration in lung compared with that of DMSO-treated mice at 6 hours after LPS injection (Fig. 8B). In addition, echocardiography analysis also found that 3PO treatment had a protective effect on cardiac function in mice with LPS challenge (Fig. S3). Given the fact that endothelial inflammation-mediated leukocyte infiltration is critical for ALI, we further investigated whether 3PO treatment could inhibit leukocyte recruitment and EC inflammation *in vivo*. Staining of lung sections with Ly6G and Mac2 showed that LPS caused a significant increase in neutrophil and macrophage infiltration at 6 hours after LPS injection, while PFKFB3 blockade with 3PO reduced the numbers of neutrophils and macrophages adhering to and migrating across ECs (Fig. 8C and 8D), indicating that 3PO decreased leukocyte recruitment into the lung. Western blot assays showed that LPS-induced Icam-1 expression was blunted in lungs of mice treated with 3PO (Fig. 8E). Furthermore,

immunostaining showed that the increased expression of Icam-1 and Vcam-1 in the ECs of pulmonary vascular wall of LPS-treated mice were strikingly suppressed by 3PO treatment (Fig. 8F and 8G). Collectively, these results indicate that 3PO protects mice from LPS induced ALI and sepsis, at least in part by inhibiting endothelial cell activation *in vivo*.

3.5. Pfkfb3 deficiency suppresses endothelial inflammation via inactivation of nuclear factor κB (NF-κB) signaling

To examine the role of PFKFB3 in the regulation of endothelial inflammation *in vitro*, we assessed the effects of PKFBF3 on adhesion molecule expression in HPAECs with both pharmacological and genetic approaches. HPAECs transfected with si*CTRL* or si*PFKFB3* were treated with LPS for 4 hours; qPCR assays showed that the mRNA levels of *ICAM-1*, *VCAM-1* and *E-selectin* were decreased in *PFKFB3* knockdown HPAECs compared with those of control cells (Fig. 9A–9C). Western blot assay showed changes at the protein level similar to those at the mRNA level (Fig. 9D). Accordingly, the number of human THP-1 monocytic cells firmly adhering to HPAECs transfected with si*PFKFB3* was significantly decreased compared with that in the control group (Fig. 9E). As leukocyte rolling and adhesion mainly occur in microcirculation, we also detected ICAM-1 and VCAM-1 expression and THP-1 adhesion in HPMVECs, the results were similar with that of HPAECs (Fig. S4). Additionally, pre-treatment with 3PO for 30 min before the addition of LPS markedly attenuated LPS-induced expression of ICAM-1 and VCAM-1 in HPAECs (Fig. 9F). Thus, both *PFKFB3* knockdown and PFKFB3 inhibition were able to decrease LPS-induced inflammation in HPAECs.

Previous studies have indicated that NF-κB is a crucial transcription factor that regulates the expression of EC adhesion molecules (47, 48), and its signaling is critically implicated in the pathogenesis of sepsis (7, 8, 49–51). Végran et al found that the glycolytic product lactate was able to stimulate NF-κB signaling in ECs (52). Therefore, we posited that NF-κB signaling might be involved in PFKFB3-regulated adhesion molecule expression. To test this, we first examined the effects of *PFKFB3* knockdown on the activation of NF-κB. As shown in Fig. 9G, NF-κB - p65 nuclear translocation induced by LPS was attenuated in *PFKFB3*-deleted HPAECs compared with that in control HPAECs, implying that *PFKFB3* knockdown prevented LPS-induced activation of NF-κB signaling. To further demonstrate the involvement of NF-κB, the effects of BAY 11–7085, a potent and specific NF-κB inhibitor (53), on PFKFB3-induced endothelial inflammation were evaluated by Western blot. PFKFB3 overexpression in HPAECs elevated the levels of ICAM-1, VCAM-1, p65, and p-p65, congruent with the idea that PFKFB3 is critical for the activation of NF-κB signaling and the expression of ICAM-1 and VCAM-1. However, these increases were significantly attenuated by BAY 11–7085 treatment, indicating that PFKFB3-regulated adhesion molecule expression through NF-κB signaling in LPS-treated HPAECs (Fig. 9H). Use of PDTC, a selective inhibitor of NF-κB signaling but structurally and mechanistically distinct from BAY11–7085 (54, 55), yielded similar results.

4. Discussion

Sepsis is one of the leading causes of mortality, and there are extremely limited therapeutic options. Multiorgan dysfunction or failure, including ALI, is a hallmark of sepsis. The acute phase of sepsis is characterized by a strong inflammatory reaction in many critical organs including lung. Recruitment of inflammatory cells into the lung or other organs needs adhesion molecule expression in ECs. The endothelial response to inflammatory mediators is to express adhesion molecules on the cell surface, including ICAM-1, VCAM-1, P-selectin and E-selectin, which results in increased rolling, adherence and transmigration of leukocytes into tissue (46). Mice that are deficient in adhesion molecules are resistant to lethality in the cecal ligation puncture (CLP)-induced sepsis model (56). Therefore, the search for novel therapeutic concepts to reduce endothelial-leukocyte interaction-mediated lung inflammation in ALI is an area of intense research.

Many studies have shown that glycolytic metabolism plays an important role in inflammation (57, 58). Glycolysis in lung is elevated in patients with ALI (35–37). Positron emission tomography (PET) has shown that ^{18}F-fluorodeoxyglucose (^{18}F-FDG) uptake in regions with inflammatory lesions were increased in ALI patients and LPS-exposed sheep (33, 59). Despite clinical studies that have shown that the serum levels of lactate are associated with outcomes in septic patients (17, 60), whether this increased glycolysis plays a causative role in the development of ALI and sepsis remains elusive. In our first set of experiments, we found that expression of the glycolytic regulator PFKFB3 was significantly upregulated in septic lung, specifically in pulmonary ECs. This may explain, at least in part, why glycolysis is increased in the lungs of ALI patients. Using EC-specific *Pfkfb3*-deficient mice, we unmasked the causative role of EC glycolysis in ALI and sepsis. Our data showed that EC–specific Pfkfb3-mediated endothelial inflammation, including enhanced adhesion molecule expression-mediated leukocyte infiltration, led to the development of ALI. Our *in vitro* study also showed that PFKFB3 deletion in cultured HPAECs markedly decreased adhesion molecule expression and monocyte adhesion to LPS-stimulated HPAECs. This is consistent with a previous report that EC Pfkfb3 hplo-deficiency downregulates endothelial adhesion molecules and then suppresses cancer cell invasion and metastasis (22). In addition, a recent study showed that silencing *PFKFB3* using siRNA decreases tumor necrosis factor alpha (TNF-α)-induced adhesion molecule expression and pro-inflammatory cytokine/chemokine production (61).

In the present study, we found that blockage of the glycolytic activator PFKFB3 by 3PO protected mice from LPS-induced sepsis in mice. 3PO treatment inhibited LPS-induced endothelial inflammation both *in vitro* and *in vivo*. This is in line with a previous study showing 3PO treatment reduced interleukin-1 beta (IL-1β)-stimulated endothelial adhesiveness to cancer cells (22). Our current study showed a causative role of endothelial PFKFB3 in endothelial inflammation and sepsis. A recent study reported that the PFKFB3 inhibitor 3PO decreased inflammation and apoptosis of alveolar epithelial cells in CLP-induced sepsis, indicating that in our LPS-induced sepsis model, in addition to PFKFB3-driven endothelial glycolysis, glycolysis in other cell types, such as epithelial cells and immune cells (62–64), might be also involved in the pathology of ALI and sepsis via

multiple mechanisms, and 3PO treatment in our study protects mice via inhibition of inflammatory and apoptosis events in other types of cells.

Endothelial PFKFB3-mediated inflammation may participate in the dysfunction of many organs. In this study, we mainly characterized the role of endothelial Pfkfb3 in ALI. However, many organs, including heart, liver, kidney and others, also suffer from septic injury, and these dysfunctional organs also contribute to sepsis-associated mortality. Endothelial Pfkfb3-mediated inflammation causes dysfunction of these organs. We have observed improved function for hearts and kidney in septic *Pfkfb3*$^{\Delta VEC}$ mice. Therefore, the increased survival rates in *Pfkfb3*$^{\Delta VEC}$ or 3PO-treated septic mice is attributed to improved function for many other organs in addition to the lung.

Mechanistically, the effect of PFKFB3 on adhesion molecule expression is related to NF-κB signaling. NF-κB is a key regulator that controls inflammation-related genes and drives the expression of adhesion molecules, including ICAM-1 and VCAM-1 (47, 48, 65). Inhibition of NF-κB activity suppresses LPS-induced inflammatory cytokine and adhesion molecule expression, reduces neutrophil influx, and prevents an LPS-induced increase in microvascular endothelial permeability (50, 65, 66). More importantly, NF-κB is highly activated in septic patients and plays a critical role in ALI (7, 8, 49–51). Our data showed that *PFKFB3* knockdown prevented LPS-induced NF-κB-p65 nuclear translocation, while *PFKFB3* overexpression resulted in activation of NF-κB signaling and expression of ICAM-1 and VCAM-1 in HPAECs. Notably, selective inhibitors of NF-κB signaling were capable of blocking PFKFB3-mediated expression of ICAM-1 and VCAM-1, indicating that PFKFB3-induced adhesion molecule expression is dependent on the activation of NF-κB signaling. The underlying mechanisms by which PFKFB3 directly controls the activation of NF-κB signaling may include the following possibilities. First, PFKFB3-driven glycolytic flux may fuel the generation of reactive oxygen species (67), an inevitable byproduct of mitochondrial electron transfer, which promotes activation of the redox-sensitive transcription factor NF-κB (30). Second, during the activation of NF-κB signaling in response to pro-inflammatory stimulation, such as LPS, most of the downstream signaling events or cellular processes consume energy. For example, LPS-induced IκB degradation is dependent on the ATP-dependent proteolytic 26S proteasome (68, 69). Given the fact that PFKFB3-driven glycolysis is the major source of ATP generation in ECs (glycolysis generates up to 85% of the total ATP content in ECs) (11), it is very likely that LPS induces PFKFB3 expression and activity to support the ATP demands for NF-κB activation. Finally, a previous study showed that the glycolytic byproduct lactate stimulates NF-κB signaling in ECs (52). The data from us and others have shown that *PFKFB3* knockdown lowered lactate levels in ECs (23, 24). Thus, lactate may also be responsible for PFKFB3-mediated activation of NF-κB activation.

5. Conclusion

In summary, this study demonstrates a critical role of the endothelial glycolytic activator PFKFB3 in LPS-induced ALI in a moue septic model using both endothelial-specific *Pfkfb3* knockout mice and the PFKFB3-specific inhibitor, 3PO. Our data show that the early induction of PFKFB3 protein expression in lung ECs causes an increase in EC glycolysis

and contributes to acute lung injury, which is associated with neutrophil and monocyte recruitment. Mechanistically, *PFKFB3* deficiency or inhibition prevents LPS-induced hyper-activation of NF-κB signaling, which results in downregulation of adhesion molecule expression in ECs. Our findings provide new insights into a previously unidentified role of EC glycolysis in ALI and sepsis *in vivo* and highlight the translational potential of targeting EC PFKFB3 in the treatment of ALI and sepsis.

Supplementary Material

Refer to Web version on PubMed Central for supplementary material.

Acknowledgement

This work was supported by grants from National Natural Science Foundation of China (81870324), the Shenzhen Science and Technology Innovation Committee (JCYJ20170810163238384, JCYJ20160525154531263, JCYJ20160506170316776, JCYJ20170412150405310, and JSGG20160608091824706), Guangdong Natural Science Foundation (2014A030312004), American Heart Association (16GRNT30510010) and the National Institutes of Health (R01HL134934, R01DK095862 and R01 HL142097).

Abbreviations

ALI	acute lung injury
LPS	lipopolysaccharide
EC	endothelial cell
HPAEC	human pulmonary artery endothelial cell
MLEC	mice lung endothelial cell
PFKFB3	6-Phosphofructo-2-Kinase/Fructose-2,6-Biphosphatase 3
PFK1	6-phosphofructo-1-kinase
F-2,6-P2	fructose-2,6-bisphophate
3PO	3-(3-pyridinyl)-1-(4-pyridinyl)-2-propen-1-one
ICAM-1	intracellular adhesion molecule-1
VCAM-1	vascular cell adhesion molecule 1
NF-κB	nuclear factor κB
PDTC	pyrrolidinedithiocarbamic acid
IL-1β	interleukin-1 beta
TNF-α	tumor necrosis factor alpha
PBS	phosphate buffered saline
PFA	paraformaldehyde

WT wild-type

References

1. Russell JA. Management of sepsis. The New England journal of medicine. 2006;355(16):1699–1713. [PubMed: 17050894]
2. Deutschman CS, Tracey KJ. Sepsis: current dogma and new perspectives. Immunity. 2014;40(4):463–475. [PubMed: 24745331]
3. Angus DC, van der Poll T. Severe sepsis and septic shock. The New England journal of medicine. 2013;369(9):840–851. [PubMed: 23984731]
4. Bosmann M, Ward PA. The inflammatory response in sepsis. Trends in immunology. 2013;34(3):129–136. [PubMed: 23036432]
5. Gentile LF, Cuenca AG, Efron PA, Ang D, Bihorac A, McKinley BA, Moldawer LL, Moore FA. Persistent inflammation and immunosuppression: a common syndrome and new horizon for surgical intensive care. The journal of trauma and acute care surgery. 2012;72(6):1491–1501. [PubMed: 22695412]
6. Yende S, D'Angelo G, Kellum JA, Weissfeld L, Fine J, Welch RD, Kong L, Carter M, Angus DC. Inflammatory markers at hospital discharge predict subsequent mortality after pneumonia and sepsis. Am J Respir Crit Care Med. 2008;177(11):1242–1247. [PubMed: 18369199]
7. Imam F, Al-Harbi NO, Al-Harbi MM, Ansari MA, Zoheir KM, Iqbal M, Anwer MK, Al Hoshani AR, Attia SM, Ahmad SF. Diosmin downregulates the expression of T cell receptors, pro-inflammatory cytokines and NF-kappaB activation against LPS-induced acute lung injury in mice. Pharmacological research. 2015;102:1–11. [PubMed: 26361726]
8. Dong J, Liao W, Tan LH, Yong A, Peh WY, Wong WSF. Gene silencing of receptor-interacting protein 2 protects against cigarette smoke-induced acute lung injury. Pharmacological research. 2019;139:560–568. [PubMed: 30394320]
9. Galley HF, Webster NR. Physiology of the endothelium. British journal of anaesthesia. 2004;93(1):105–113. [PubMed: 15121728]
10. Aird WC. The role of the endothelium in severe sepsis and multiple organ dysfunction syndrome. Blood. 2003;101(10):3765–3777. [PubMed: 12543869]
11. De Bock K, Georgiadou M, Schoors S, Kuchnio A, Wong BW, Cantelmo AR, Quaegebeur A, Ghesquiere B, Cauwenberghs S, Eelen G, Phng LK, Betz I, Tembuyser B, Brepoels K, Welti J, Geudens I, Segura I, Cruys B, Bifari F, Decimo I, Blanco R, Wyns S, Vangindertael J, Rocha S, Collins RT, Munck S, Daelemans D, Imamura H, Devlieger R, Rider M, Van Veldhoven PP, Schuit F, Bartrons R, Hofkens J, Fraisl P, Telang S, Deberardinis RJ, Schoonjans L, Vinckier S, Chesney J, Gerhardt H, Dewerchin M, Carmeliet P. Role of PFKFB3-driven glycolysis in vessel sprouting. Cell. 2013;154(3):651–663. [PubMed: 23911327]
12. Eelen G, de Zeeuw P, Treps L, Harjes U, Wong BW, Carmeliet P. Endothelial Cell Metabolism. Physiological reviews. 2018;98(1):3–58. [PubMed: 29167330]
13. Van Wyngene L, Vandewalle J, Libert C. Reprogramming of basic metabolic pathways in microbial sepsis: therapeutic targets at last? EMBO molecular medicine. 2018;10(8).
14. Shapiro NI, Howell MD, Talmor D, Nathanson LA, Lisbon A, Wolfe RE, Weiss JW. Serum lactate as a predictor of mortality in emergency department patients with infection. Annals of emergency medicine. 2005;45(5):524–528. [PubMed: 15855951]
15. Wong HR, Lindsell CJ, Pettila V, Meyer NJ, Thair SA, Karlsson S, Russell JA, Fjell CD, Boyd JH, Ruokonen E, Shashaty MG, Christie JD, Hart KW, Lahni P, Walley KR. A multibiomarker-based outcome risk stratification model for adult septic shock*. Crit Care Med. 2014;42(4):781–789. [PubMed: 24335447]
16. Nguyen HB, Rivers EP, Knoblich BP, Jacobsen G, Muzzin A, Ressler JA, Tomlanovich MC. Early lactate clearance is associated with improved outcome in severe sepsis and septic shock. Crit Care Med. 2004;32(8):1637–1642. [PubMed: 15286537]
17. Mikkelsen ME, Miltiades AN, Gaieski DF, Goyal M, Fuchs BD, Shah CV, Bellamy SL, Christie JD. Serum lactate is associated with mortality in severe sepsis independent of organ failure and shock. Crit Care Med. 2009;37(5):1670–1677. [PubMed: 19325467]

18. Weber G Enzymology of cancer cells (second of two parts). The New England journal of medicine. 1977;296(10):541–551. [PubMed: 189189]

19. Van Schaftingen E, Jett MF, Hue L, Hers HG. Control of liver 6-phosphofructokinase by fructose 2,6-bisphosphate and other effectors. Proc Natl Acad Sci U S A. 1981;78(6):3483–3486. [PubMed: 6455662]

20. Sakakibara R, Kato M, Okamura N, Nakagawa T, Komada Y, Tominaga N, Shimojo M, Fukasawa M. Characterization of a human placental fructose-6-phosphate, 2-kinase/fructose-2,6-bisphosphatase. Journal of biochemistry. 1997;122(1):122–128. [PubMed: 9276680]

21. Rider MH, Bertrand L, Vertommen D, Michels PA, Rousseau GG, Hue L. 6-phosphofructo-2-kinase/fructose-2,6-bisphosphatase: head-to-head with a bifunctional enzyme that controls glycolysis. The Biochemical journal. 2004;381(Pt 3):561–579. [PubMed: 15170386]

22. Cantelmo AR, Conradi LC, Brajic A, Goveia J, Kalucka J, Pircher A, Chaturvedi P, Hol J, Thienpont B, Teuwen LA, Schoors S, Boeckx B, Vriens J, Kuchnio A, Veys K, Cruys B, Finotto L, Treps L, Stav-Noraas TE, Bifari F, Stapor P, Decimo I, Kampen K, De Bock K, Haraldsen G, Schoonjans L, Rabelink T, Eelen G, Ghesquiere B, Rehman J, Lambrechts D, Malik AB, Dewerchin M, Carmeliet P. Inhibition of the Glycolytic Activator PFKFB3 in Endothelium Induces Tumor Vessel Normalization, Impairs Metastasis, and Improves Chemotherapy. Cancer Cell. 2016;30(6):968–985. [PubMed: 27866851]

23. Schoors S, De Bock K, Cantelmo AR, Georgiadou M, Ghesquiere B, Cauwenberghs S, Kuchnio A, Wong BW, Quaegebeur A, Goveia J, Bifari F, Wang X, Blanco R, Tembuyser B, Cornelissen I, Bouche A, Vinckier S, Diaz-Moralli S, Gerhardt H, Telang S, Cascante M, Chesney J, Dewerchin M, Carmeliet P. Partial and transient reduction of glycolysis by PFKFB3 blockade reduces pathological angiogenesis. Cell Metab. 2014;19(1):37–48. [PubMed: 24332967]

24. Xu Y, An X, Guo X, Habtetsion TG, Wang Y, Xu X, Kandala S, Li Q, Li H, Zhang C, Caldwell RB, Fulton DJ, Su Y, Hoda MN, Zhou G, Wu C, Huo Y. Endothelial PFKFB3 plays a critical role in angiogenesis. Arterioscler Thromb Vasc Biol. 2014;34(6):1231–1239. [PubMed: 24700124]

25. Mirzapoiazova T, Kolosova IA, Moreno L, Sammani S, Garcia JG, Verin AD. Suppression of endotoxin-induced inflammation by taxol. Eur Respir J. 2007;30(3):429–435. [PubMed: 17537765]

26. Wu Y, Wang L, Meng L, Cao GK, Zhao YL, Zhang Y. Biological effects of autophagy in mice with sepsis-induced acute kidney injury. Experimental and therapeutic medicine. 2019;17(1):316–322. [PubMed: 30651797]

27. Liu Z, Yan S, Wang J, Xu Y, Wang Y, Zhang S, Xu X, Yang Q, Zeng X, Zhou Y, Gu X, Lu S, Fu Z, Fulton DJ, Weintraub NL, Caldwell RB, Zhang W, Wu C, Liu XL, Chen JF, Ahmad A, Kaddour-Djebbar I, Al-Shabrawey M, Li Q, Jiang X, Sun Y, Sodhi A, Smith L, Hong M, Huo Y. Endothelial adenosine A2a receptor-mediated glycolysis is essential for pathological retinal angiogenesis. Nat Commun. 2017;8(1):584. [PubMed: 28928465]

28. Liu Z, Wang J, Huang E, Gao S, Li H, Lu J, Tian K, Little PJ, Shen X, Xu S, Liu P. Tanshinone IIA suppresses cholesterol accumulation in human macrophages: role of heme oxygenase-1. Journal of lipid research. 2014;55(2):201–213. [PubMed: 24302760]

29. Van Schaftingen E, Lederer B, Bartrons R, Hers HG. A kinetic study of pyrophosphate: fructose-6-phosphate phosphotransferase from potato tubers. Application to a microassay of fructose 2,6-bisphosphate. European journal of biochemistry. 1982;129(1):191–195. [PubMed: 6297885]

30. Liu Z, Xu S, Huang X, Wang J, Gao S, Li H, Zhou C, Ye J, Chen S, Jin ZG, Liu P. Cryptotanshinone, an orally bioactive herbal compound from Danshen, attenuates atherosclerosis in apolipoprotein E-deficient mice: role of lectin-like oxidized LDL receptor-1 (LOX-1). Br J Pharmacol. 2015;172(23):5661–5675. [PubMed: 25572313]

31. Liu Z, Wang J, Huang X, Li Z, Liu P. Deletion of sirtuin 6 accelerates endothelial dysfunction and atherosclerosis in apolipoprotein E-deficient mice. Transl Res. 2016;172:18–29.e12. [PubMed: 26924042]

32. Bellani G, Messa C, Guerra L, Spagnolli E, Foti G, Patroniti N, Fumagalli R, Musch G, Fazio F, Pesenti A. Lungs of patients with acute respiratory distress syndrome show diffuse inflammation in normally aerated regions: a [18F]-fluoro-2-deoxy-D-glucose PET/CT study. Crit Care Med. 2009;37(7):2216–2222. [PubMed: 19487931]

33. Bellani G, Guerra L, Musch G, Zanella A, Patroniti N, Mauri T, Messa C, Pesenti A. Lung regional metabolic activity and gas volume changes induced by tidal ventilation in patients with acute lung injury. Am J Respir Crit Care Med. 2011;183(9):1193–1199. [PubMed: 21257791]
34. Musch G, Venegas JG, Bellani G, Winkler T, Schroeder T, Petersen B, Harris RS, Melo MF. Regional gas exchange and cellular metabolic activity in ventilator-induced lung injury. Anesthesiology. 2007;106(4):723–735. [PubMed: 17413910]
35. Brown SD, Clark C, Gutierrez G. Pulmonary lactate release in patients with sepsis and the adult respiratory distress syndrome. Journal of critical care. 1996;11(1):2–8. [PubMed: 8904278]
36. Douzinas EE, Tsidemiadou PD, Pitaridis MT, Andrianakis I, Bobota-Chloraki A, Katsouyanni K, Sfyras D, Malagari K, Roussos C. The regional production of cytokines and lactate in sepsis-related multiple organ failure. Am J Respir Crit Care Med. 1997;155(1):53–59. [PubMed: 9001289]
37. De Backer D, Creteur J, Zhang H, Norrenberg M, Vincent JL. Lactate production by the lungs in acute lung injury. Am J Respir Crit Care Med. 1997;156(4 Pt 1):1099–1104. [PubMed: 9351608]
38. Maniatis NA, Kotanidou A, Catravas JD, Orfanos SE. Endothelial pathomechanisms in acute lung injury. Vascular pharmacology. 2008;49(4–6):119–133. [PubMed: 18722553]
39. Li FL, Liu JP, Bao RX, Yan G, Feng X, Xu YP, Sun YP, Yan W, Ling ZQ, Xiong Y, Guan KL, Yuan HX. Acetylation accumulates PFKFB3 in cytoplasm to promote glycolysis and protects cells from cisplatin-induced apoptosis. Nat Commun. 2018;9(1):508. [PubMed: 29410405]
40. Jiang H, Shi H, Sun M, Wang Y, Meng Q, Guo P, Cao Y, Chen J, Gao X, Li E, Liu J. PFKFB3-Driven Macrophage Glycolytic Metabolism Is a Crucial Component of Innate Antiviral Defense. J Immunol. 2016;197(7):2880–2890. [PubMed: 27566823]
41. Maniatis NA, Orfanos SE. The endothelium in acute lung injury/acute respiratory distress syndrome. Current opinion in critical care. 2008;14(1):22–30. [PubMed: 18195622]
42. Abraham E Neutrophils and acute lung injury. Crit Care Med. 2003;31(4 Suppl):S195–199. [PubMed: 12682440]
43. Reutershan J, Basit A, Galkina EV, Ley K. Sequential recruitment of neutrophils into lung and bronchoalveolar lavage fluid in LPS-induced acute lung injury. Am J Physiol Lung Cell Mol Physiol. 2005;289(5):L807–815. [PubMed: 15951336]
44. Razavi HM, Wang le F, Weicker S, Rohan M, Law C, McCormack DG, Mehta S. Pulmonary neutrophil infiltration in murine sepsis: role of inducible nitric oxide synthase. Am J Respir Crit Care Med. 2004;170(3):227–233. [PubMed: 15059787]
45. Johnston LK, Rims CR, Gill SE, McGuire JK, Manicone AM. Pulmonary macrophage subpopulations in the induction and resolution of acute lung injury. American journal of respiratory cell and molecular biology. 2012;47(4):417–426. [PubMed: 22721830]
46. Laudes IJ, Guo RF, Riedemann NC, Speyer C, Craig R, Sarma JV, Ward PA. Disturbed homeostasis of lung intercellular adhesion molecule-1 and vascular cell adhesion molecule-1 during sepsis. Am J Pathol. 2004;164(4):1435–1445. [PubMed: 15039231]
47. Ledebur HC, Parks TP. Transcriptional regulation of the intercellular adhesion molecule-1 gene by inflammatory cytokines in human endothelial cells. Essential roles of a variant NF-kappa B site and p65 homodimers. J Biol Chem. 1995;270(2):933–943. [PubMed: 7822333]
48. Pahl HL. Activators and target genes of Rel/NF-kappaB transcription factors. Oncogene. 1999;18(49):6853–6866. [PubMed: 10602461]
49. Arnalich F, Garcia-Palomero E, Lopez J, Jimenez M, Madero R, Renart J, Vazquez JJ, Montiel C. Predictive value of nuclear factor kappaB activity and plasma cytokine levels in patients with sepsis. Infect Immun. 2000;68(4):1942–1945. [PubMed: 10722586]
50. Liu SF, Ye X, Malik AB. Pyrrolidine dithiocarbamate prevents I-kappaB degradation and reduces microvascular injury induced by lipopolysaccharide in multiple organs. Molecular pharmacology. 1999;55(4):658–667. [PubMed: 10101023]
51. Fan J, Ye RD, Malik AB. Transcriptional mechanisms of acute lung injury. Am J Physiol Lung Cell Mol Physiol. 2001;281(5):L1037–1050. [PubMed: 11597894]
52. Vegran F, Boidot R, Michiels C, Sonveaux P, Feron O. Lactate influx through the endothelial cell monocarboxylate transporter MCT1 supports an NF-kappaB/IL-8 pathway that drives tumor angiogenesis. Cancer Res. 2011;71(7):2550–2560. [PubMed: 21300765]

53. Pierce JW, Schoenleber R, Jesmok G, Best J, Moore SA, Collins T, Gerritsen ME. Novel inhibitors of cytokine-induced IkappaBalpha phosphorylation and endothelial cell adhesion molecule expression show anti-inflammatory effects in vivo. J Biol Chem. 1997;272(34):21096–21103. [PubMed: 9261113]
54. Schreck R, Meier B, Mannel DN, Droge W, Baeuerle PA. Dithiocarbamates as potent inhibitors of nuclear factor kappa B activation in intact cells. J Exp Med. 1992;175(5):1181–1194. [PubMed: 1314883]
55. Nemeth ZH, Deitch EA, Szabo C, Hasko G. Pyrrolidinedithiocarbamate inhibits NF-kappaB activation and IL-8 production in intestinal epithelial cells. Immunology letters. 2003;85(1):41–46. [PubMed: 12505195]
56. Matsukawa A, Lukacs NW, Hogaboam CM, Knibbs RN, Bullard DC, Kunkel SL, Stoolman LM. Mice genetically lacking endothelial selectins are resistant to the lethality in septic peritonitis. Experimental and molecular pathology. 2002;72(1):68–76. [PubMed: 11784125]
57. Cheng SC, Joosten LA, Netea MG. The interplay between central metabolism and innate immune responses. Cytokine & growth factor reviews. 2014;25(6):707–713. [PubMed: 25001414]
58. Cheng SC, Scicluna BP, Arts RJ, Gresnigt MS, Lachmandas E, Giamarellos-Bourboulis EJ, Kox M, Manjeri GR, Wagenaars JA, Cremer OL, Leentjens J, van der Meer AJ, van de Veerdonk FL, Bonten MJ, Schultz MJ, Willems PH, Pickkers P, Joosten LA, van der Poll T, Netea MG. Broad defects in the energy metabolism of leukocytes underlie immunoparalysis in sepsis. Nat Immunol. 2016;17(4):406–413. [PubMed: 26950237]
59. Wellman TJ, Winkler T, Costa EL, Musch G, Harris RS, Zheng H, Venegas JG, Vidal Melo MF. Effect of local tidal lung strain on inflammation in normal and lipopolysaccharide-exposed sheep*. Crit Care Med. 2014;42(7):e491–500. [PubMed: 24758890]
60. Chertoff J, Chisum M, Garcia B, Lascano J. Lactate kinetics in sepsis and septic shock: a review of the literature and rationale for further research. Journal of intensive care. 2015;3:39. [PubMed: 26445673]
61. Zhang R, Li R, Liu Y, Li L, Tang Y. The Glycolytic Enzyme PFKFB3 Controls TNF-alpha-Induced Endothelial Proinflammatory Responses. Inflammation. 2018.
62. Gong Y, Lan H, Yu Z, Wang M, Wang S, Chen Y, Rao H, Li J, Sheng Z, Shao J. Blockage of glycolysis by targeting PFKFB3 alleviates sepsis-related acute lung injury via suppressing inflammation and apoptosis of alveolar epithelial cells. Biochem Biophys Res Commun. 2017;491(2):522–529. [PubMed: 28576491]
63. Yang L, Xie M, Yang M, Yu Y, Zhu S, Hou W, Kang R, Lotze MT, Billiar TR, Wang H, Cao L, Tang D. PKM2 regulates the Warburg effect and promotes HMGB1 release in sepsis. Nat Commun. 2014;5:4436. [PubMed: 25019241]
64. Xie M, Yu Y, Kang R, Zhu S, Yang L, Zeng L, Sun X, Yang M, Billiar TR, Wang H, Cao L, Jiang J, Tang D. PKM2-dependent glycolysis promotes NLRP3 and AIM2 inflammasome activation. Nat Commun. 2016;7:13280. [PubMed: 27779186]
65. Liu SF, Ye X, Malik AB. Inhibition of NF-kappaB activation by pyrrolidine dithiocarbamate prevents In vivo expression of proinflammatory genes. Circulation. 1999;100(12):1330–1337. [PubMed: 10491379]
66. Liu SF, Malik AB. NF-kappa B activation as a pathological mechanism of septic shock and inflammation. Am J Physiol Lung Cell Mol Physiol. 2006;290(4):L622–l645. [PubMed: 16531564]
67. Shirai T, Nazarewicz RR, Wallis BB, Yanes RE, Watanabe R, Hilhorst M, Tian L, Harrison DG, Giacomini JC, Assimes TL, Goronzy JJ, Weyand CM. The glycolytic enzyme PKM2 bridges metabolic and inflammatory dysfunction in coronary artery disease. J Exp Med. 2016;213(3):337–354. [PubMed: 26926996]
68. Alkalay I, Yaron A, Hatzubai A, Orian A, Ciechanover A, Ben-Neriah Y. Stimulation-dependent I kappa B alpha phosphorylation marks the NF-kappa B inhibitor for degradation via the ubiquitin-proteasome pathway. Proc Natl Acad Sci U S A. 1995;92(23):10599–10603. [PubMed: 7479848]
69. Chen Z, Hagler J, Palombella VJ, Melandri F, Scherer D, Ballard D, Maniatis T. Signal-induced site-specific phosphorylation targets I kappa B alpha to the ubiquitin-proteasome pathway. Genes & development. 1995;9(13):1586–1597. [PubMed: 7628694]

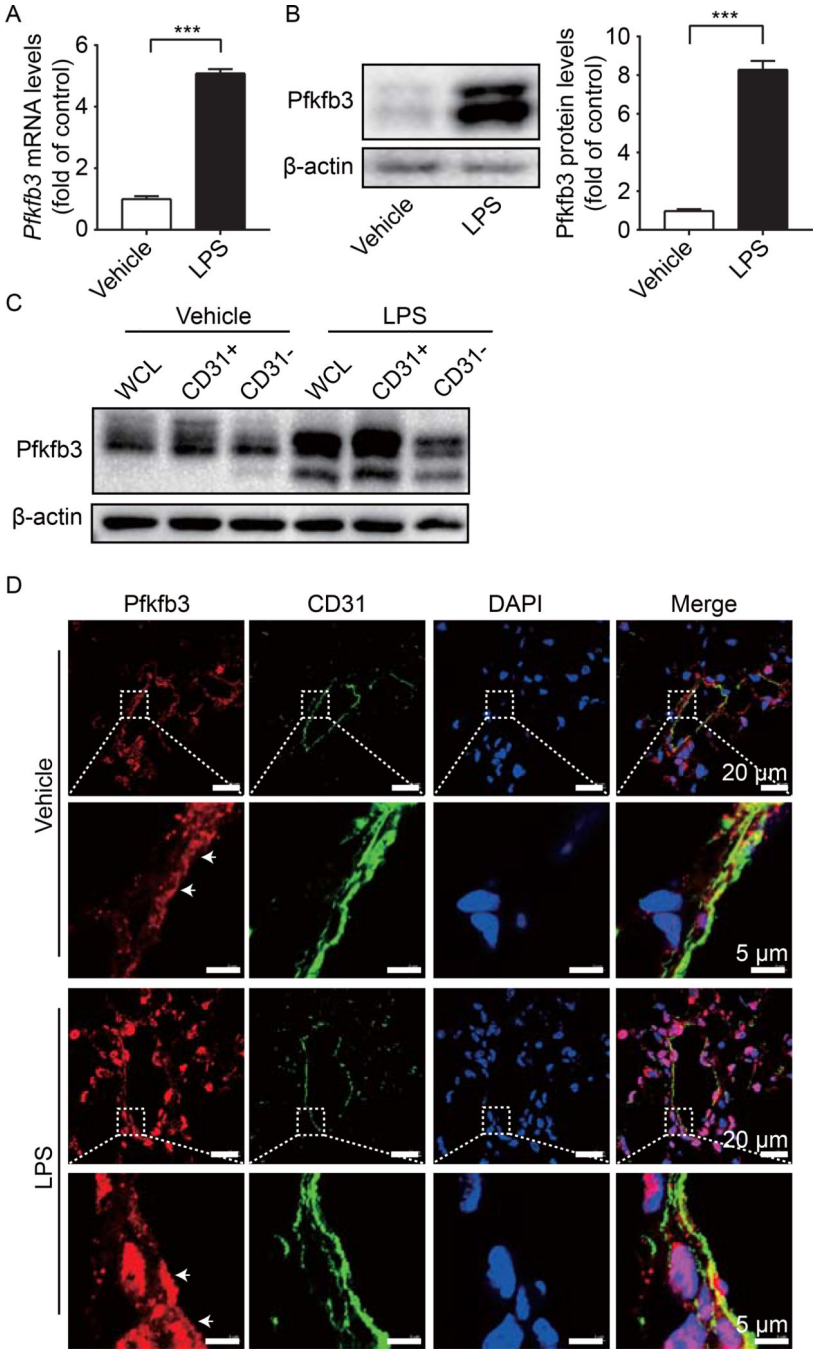

Fig. 1. Pfkfb3 expression in lung ECs is increased in LPS-induced ALI.

(**A**) Real time-PCR analysis of *Pfkfb3* mRNA levels in the lung homogenates of control or LPS-challenged mice. n = 6. (**B**) Western blot analysis and densitometric quantification of Pfkfb3 protein levels in the lung lysates of control and LPS-injected mice. n = 6. (**C**) Western blot analysis of Pfkfb3 protein levels in whole cell lysate (WCL), CD31-positive (CD31+) and CD31-negative cells (CD31-) in the lung samples of control or LPS-treated mice. (**D**) Representative micrographs of Pfkfb3 expression in the pulmonary endothelium of control or LPS-challenged mice. Sections were co-stained for Pfkfb3 (red), CD31 (green)

and DAPI (blue). Data are represented as means ± SEM. Statistical significance was determined by unpaired Student's *t* test, *** $p < 0.001$.

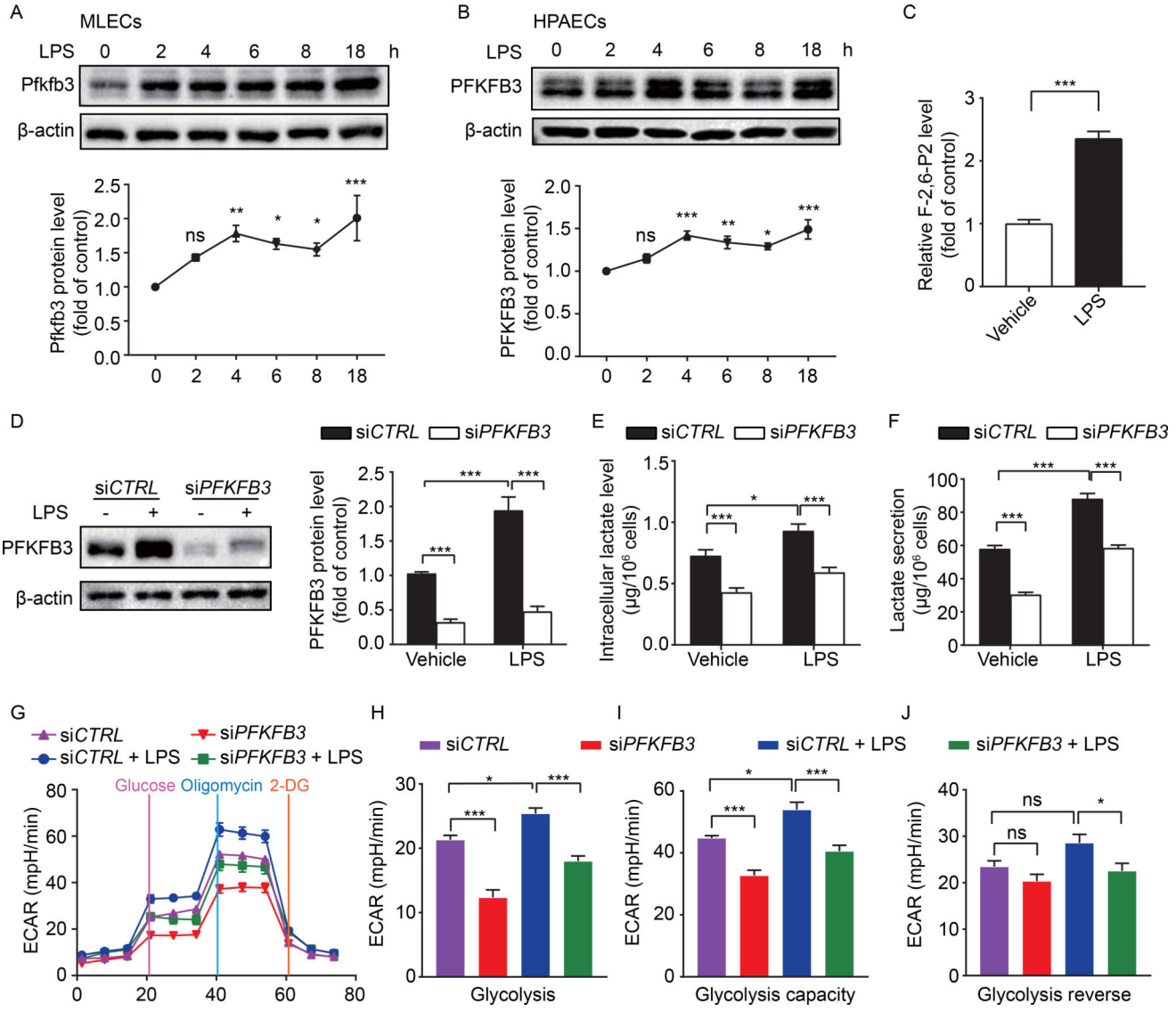

Fig. 2. PFKFB3 enhances glycolysis in LPS-treated lung ECs.

(**A-B**) Western blot analysis and densitometric quantification of PFKFB3 protein levels in MLECs (**A**) and HPAECs (**B**) following 1 μg/mL LPS treatment for indicated time. n = 5. (**C**) Relative F-2,6-P2 levels in HPAECs treated with vehicle or 1 μg/mL LPS for 4 h. n = 9. (**D**) Western blot analysis and densitometric quantification of PFKFB3 protein levels in si*CTRL* or si*PFKFB3*-transfected HPAECs with treatment of vehicle or 1 μg/mL LPS for 4 hours. n = 5. (**E-F**) Levels of intracellular lactate (**E**) and secreted lactate (**F**) of HPAECs transfected with si*CTRL* or si*PFKFB3* with treatment of vehicle or 1 μg/mL LPS for 4 h. n = 6. (**G**) ECAR profile showing glycolytic function in si*CTRL* or si*PFKFB3*-transfected HPAECs with treatment of vehicle or 1 μg/mL LPS for 4 h. Vertical lines indicate the time of addition of glucose (10 mmol/L), oligomycin (2 μmol/L), and 2-DG (50 mmol/L). (**H-J**) Quantification of glycolysis (**H**), glycolysis capacity (**I**), and glycolysis reserve (**J**) from G. n = 6 for HPAECs transfected with si*CTRL* followed by treatment with vehicle, n = 8 for the other three groups. Data are represented as means ± SEM. Statistical significance was

determined by one-way ANOVA followed by Bonferroni test. *$p < 0.05$ was considered significant, ** $p < 0.01$, *** $p < 0.001$.

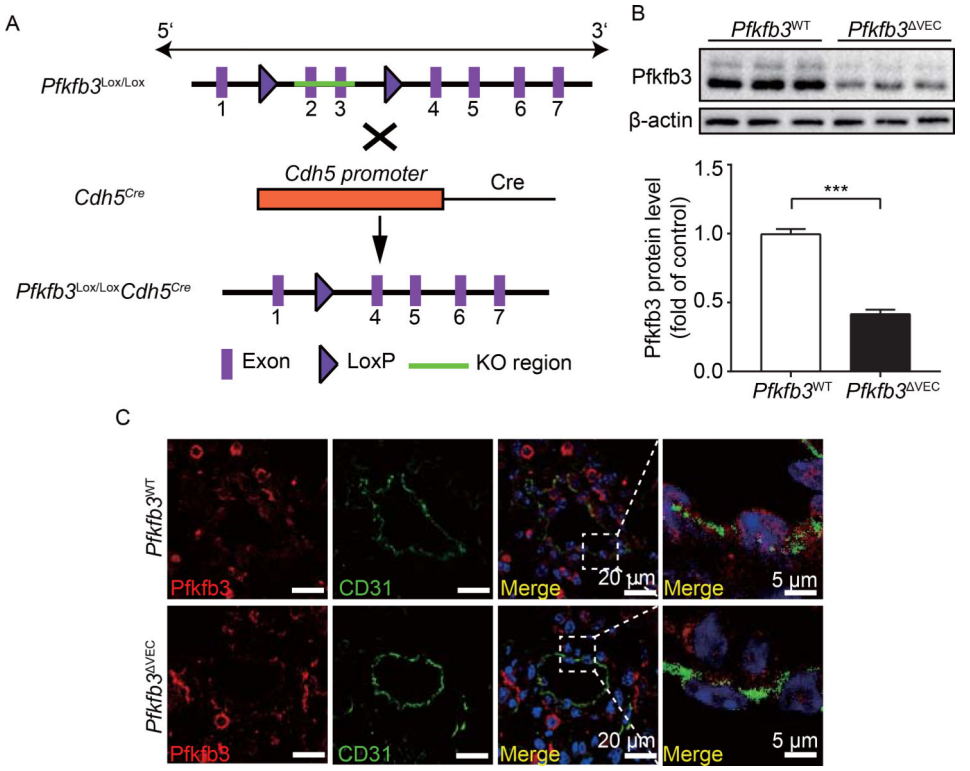

Fig. 3. Generation and characterization of *Pfkfb3*$^{\Delta VEC}$ mice.

(**A**) Schematic diagram of endothelial-specific *Pfkfb3*-deficient mouse generation. (**B**) Western blot analysis and densitometric quantification of Pfkfb3 protein levels in MLECs of *Pfkfb3*^{WT} and *Pfkfb3*$^{\Delta VEC}$ mice. n = 6. (**C**) Representative images of Pfkfb3 localization in the lung sections of *Pfkfb3*^{WT} and *Pfkfb3*$^{\Delta VEC}$ mice. Sections were co-stained for Pfkfb3 (red), CD31 (green) and DAPI (blue). Data are represented as means ± SEM. Statistical significance was determined by unpaired Student's *t* test, *** $p < 0.001$.

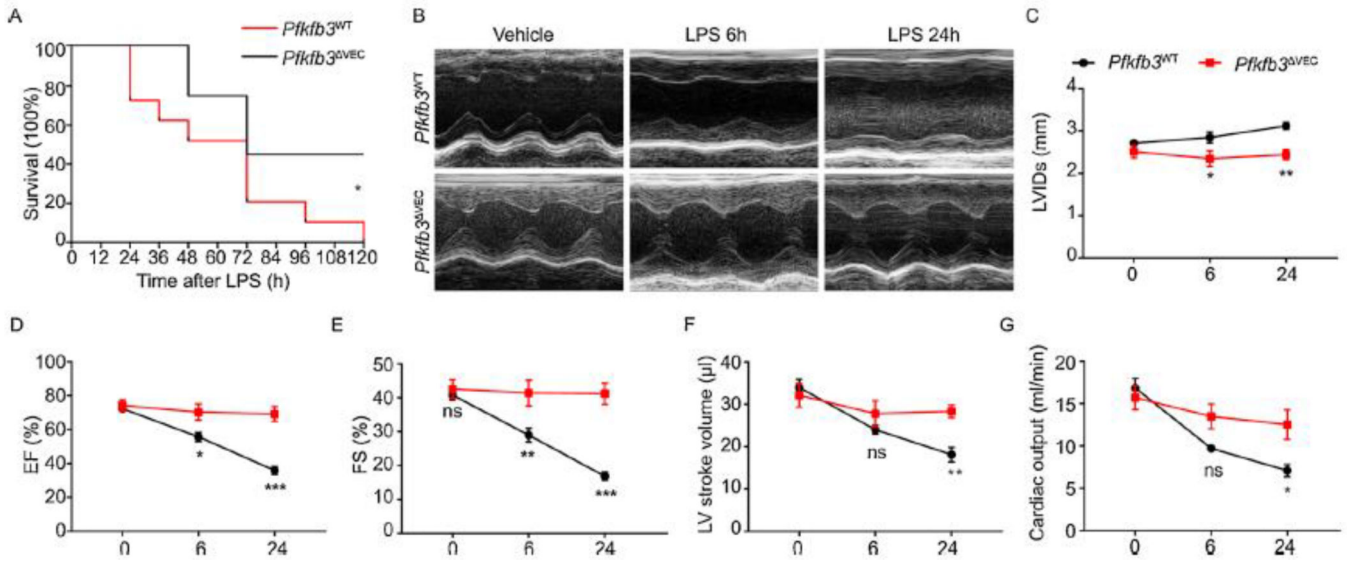

Fig. 4. Endothelial-specific *Pfkfb3* deficiency protects mice from LPS-induced endotoxemia.

(**A**) Mortality of *Pfkfb3*^{WT} and *Pfkfb3*$^{\Delta VEC}$ mice after LPS administration. Mice were injected intraperitoneally (i.p.) with LPS at a dose of 12.5 mg/kg body weight and were monitored for 10 d after LPS challenge. n =10 mice per group. Statistical analysis was performed using log-rank test, *$p < 0.05$ was considered significant. (**B**) Representative M-mode echocardiograms show improved cardiac function in *Pfkfb3*$^{\Delta VEC}$ mice exposed to 6 mg/kg LPS compared with *Pfkfb3*^{WT} mice. (**C-G**) Quantification of left ventricle (LV) systolic (s) internal diameters (LVIDs, mm; **C**), ejection fraction (EF %; **D**), fractional shortening (FS %; **E**), LV stroke volume (µl; **F**), and cardiac output (ml/min; **G**). n = 5–8 mice per group. Data are represented as mean ± SEM. Statistical significance was determined by one-way ANOVA followed by Bonferroni test. *$p < 0.05$ was considered significant, ** $p < 0.01$, *** $p < 0.001$.

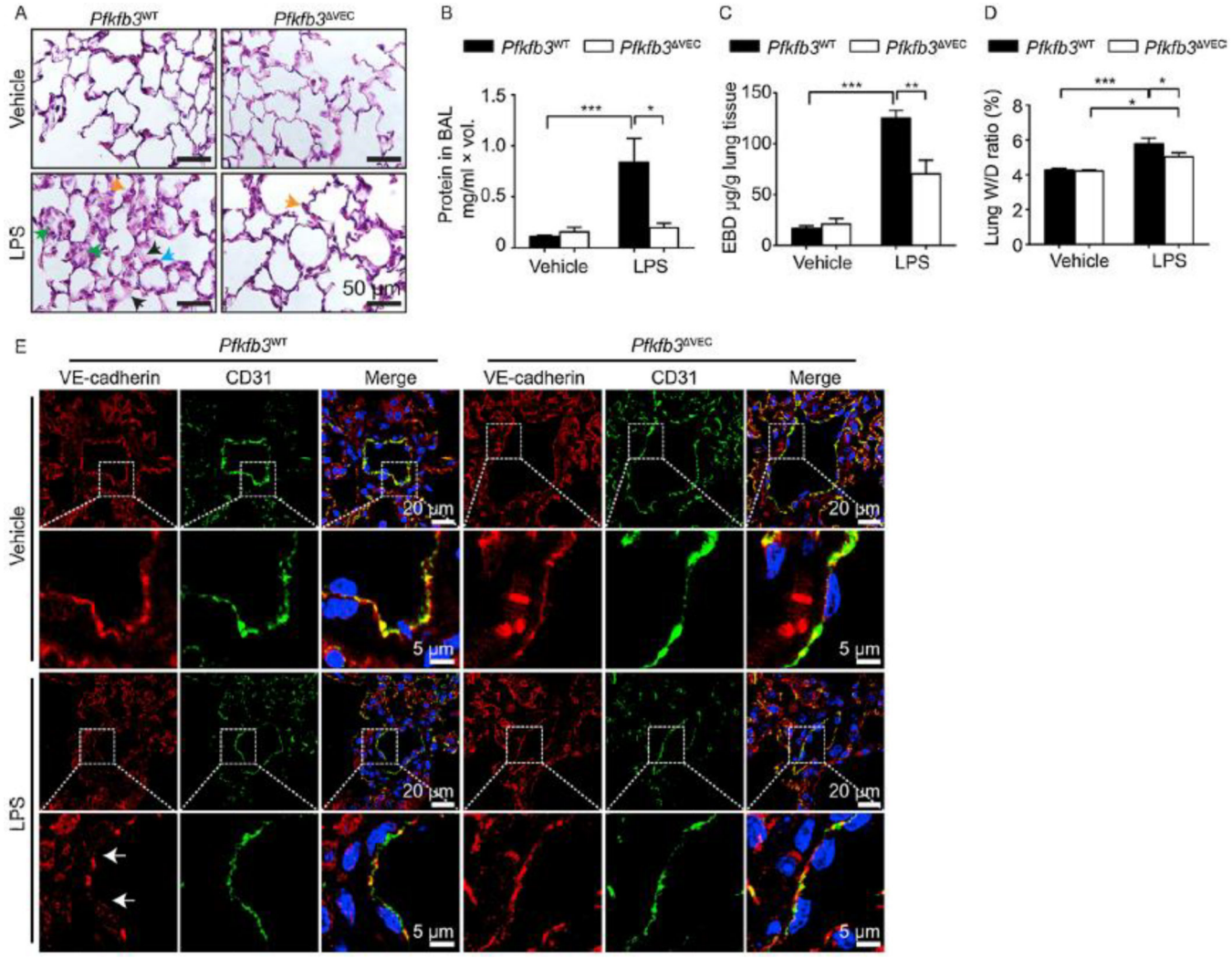

Fig. 5. Endothelial-specific *Pfkfb3* deficiency protects mice from LPS-induced ALI.

(**A**) Representative images of hematoxylin and eosin staining of lung sections from *Pfkfb3*^{WT} and *Pfkfb3*$^{\Delta VEC}$ mice exposed to vehicle or 12.5 mg/kg LPS for 6 hours. Scale bars, 50 μm. Green arrows indicate neutrophils in the alveolar space, yellow arrows indicate neutrophils in the interstitial space, black arrows indicates hyaline membranes, and blue arrows indicate thickening of the alveolar walls. (**B**) Total protein accumulation in bronchioalveolar lavage fluid (BALF) of mice treated with vehicle or 1 mg/kg LPS intratracheally (i.t.) for 6 hours. n = 4. (**C**) Quantitative analysis of Evan blue dry (EBD) extravasation of the lung from *Pfkfb3*^{WT} mice and *Pfkfb3*$^{\Delta VEC}$ mice after vehicle or 1 mg/kg LPS injection by i.t. for 6 hours. The EBA content of lung extracts was determined spectrophotometrically. n = 4. (**D**) The wet-to-dry (W/D) ratio of lung tissue from *Pfkfb3*^{WT} and *Pfkfb3*$^{\Delta VEC}$ mice after LPS challenge for 6 hours. n = 5. Data are presented as means ± SEM. Statistical significance was determined by one-way ANOVA followed by Bonferroni test. *$p < 0.05$ was considered significant, ** $p < 0.01$, *** $p < 0.001$. (**E**) Representative micrographs of VE-cadherin staining in the pulmonary endothelial of *Pfkfb3*^{WT} and

Pfkfb3$^{\Delta VEC}$ mice challenged with vehicle or 12.5 mg/kg LPS for 6 hours. Sections were co-stained for VE-cadherin (red), CD31 (green) and DAPI (blue). Scale bar, 20 μm or 5 μm.

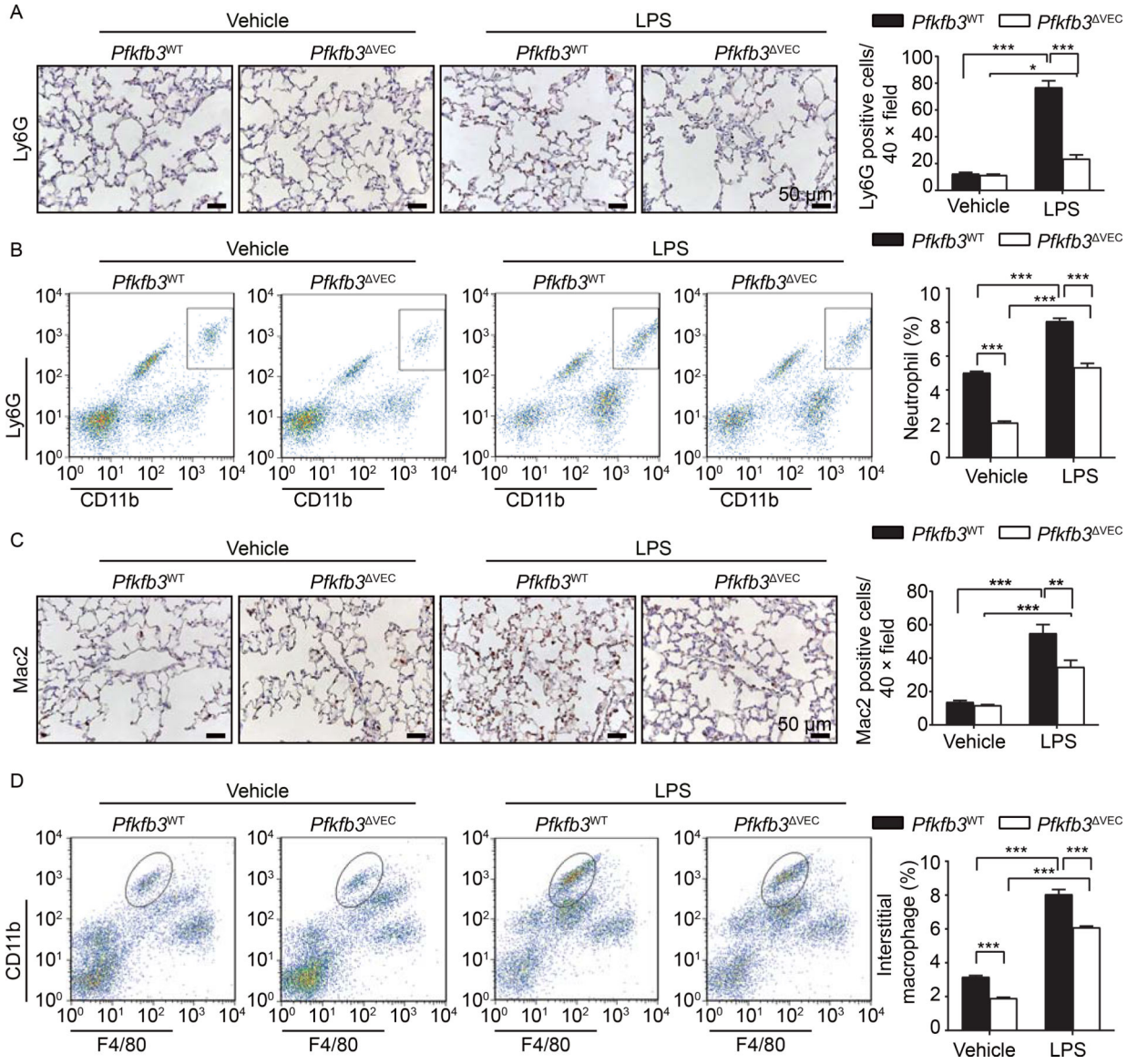

Fig. 6. Endothelial-specific *Pfkfb3* deficiency decreases neutrophil and monocyte infiltration into the lung.

(**A**) Representative images and quantification for immunohistochemical staining of the neutrophil marker Ly6G in lung sections from vehicle or LPS-treated *Pfkfb3*^{WT} and *Pfkfb3*$^{\Delta VEC}$ mice. Scale bar, 50 μm. n = 6. (**B**) Flow cytometric analysis of CD11b$^+$/Ly6G$^+$ neutrophils within the CD45$^+$ gated cells in the lung. n = 6. (**C**) Representative images and quantification for immunohistochemical staining of the macrophage marker Mac2 in lung sections from vehicle or LPS-treated *Pfkfb3*^{WT} and *Pfkfb3*$^{\Delta VEC}$ mice. Scale bar, 50 μm. n = 6. (**D**) Flow cytometric analysis of CD11b$^+$/F4/80$^+$ macrophages within the CD45$^+$ gated cells in the lung. n = 6. Data are represented as means ± SEM. Statistical significance was determined by one-way ANOVA followed by Bonferroni test. *$p < 0.05$ was considered significant, ** $p < 0.01$, *** $p < 0.001$.

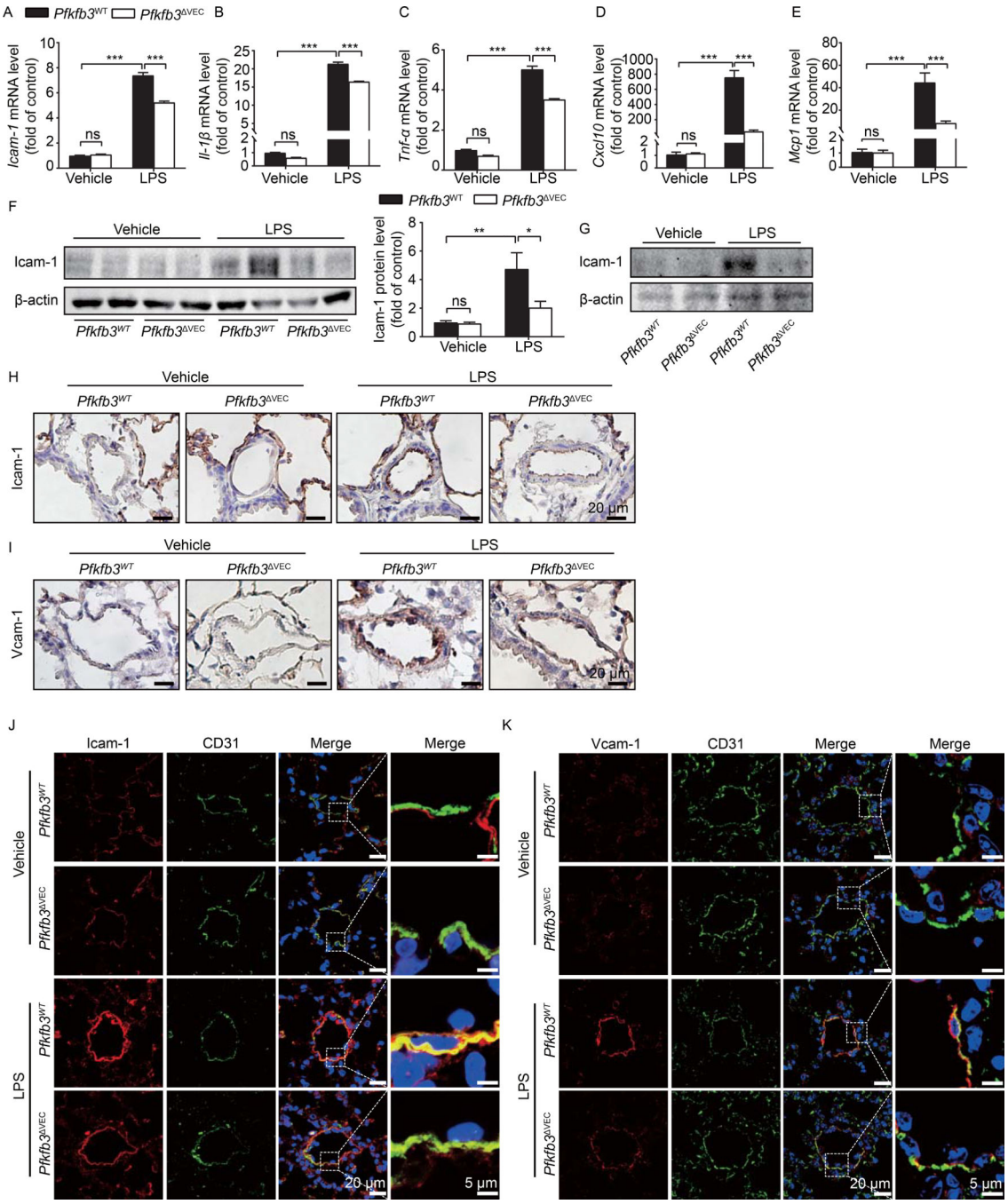

Fig. 7. Endothelial specific *Pfkfb3* deficiency decreases adhesion molecule expression in the lung of LPS-treated mice.

(**A-E**) Real time-PCR analysis of *Icam-1* (**A**), *Il-1β* (**B**), *Tnf-α* (**C**), *Cxcl10* (**D**), and *Mcp1* (**E**) mRNA levels in mice lung ECs of *Pfkfb3*^{WT} and *Pfkfb3*$^{\Delta VEC}$ mice challenged with vehicle or 12.5 mg/kg LPS for 6 hours. (**F**) Western blot and densitometric quantification analysis of Icam-1 expression in lung homogenates of *Pfkfb3*^{WT} and *Pfkfb3*$^{\Delta VEC}$ mice challenged with vehicle or 12.5 mg/kg LPS for 6 hours. n = 6. (**G**) Western blot analysis of Icam-1 expression in isolated MLECs in *Pfkfb3*^{WT} and *Pfkfb3*$^{\Delta VEC}$ mice challenged with

vehicle or 12.5 mg/kg LPS for 6 hours. n = 4. (**H and I**) Representative images for immunohistochemical staining of Icam-1 (**H**) and Vcam-1 (**I**) in lung sections from LPS-treated *Pfkfb3*^{WT} and *Pfkfb3*$^{\Delta VEC}$ mice. Scale bar, 20 μm. (**J and K**) Representative micrographs of Icam-1 (**J**) and Vcam-1 (**K**) expression in the pulmonary endothelium of *Pfkfb3*^{WT} and *Pfkfb3*$^{\Delta VEC}$ mice challenged with vehicle or 12.5 mg/kg LPS for 6 hours. Sections were co-stained for Icam-1 (red), CD31 (green) and DAPI (blue). Data are represented as means ± SEM. Statistical significance was determined by one-way ANOVA followed by Bonferroni test. *$p < 0.05$ was considered significant, ** $p < 0.01$.

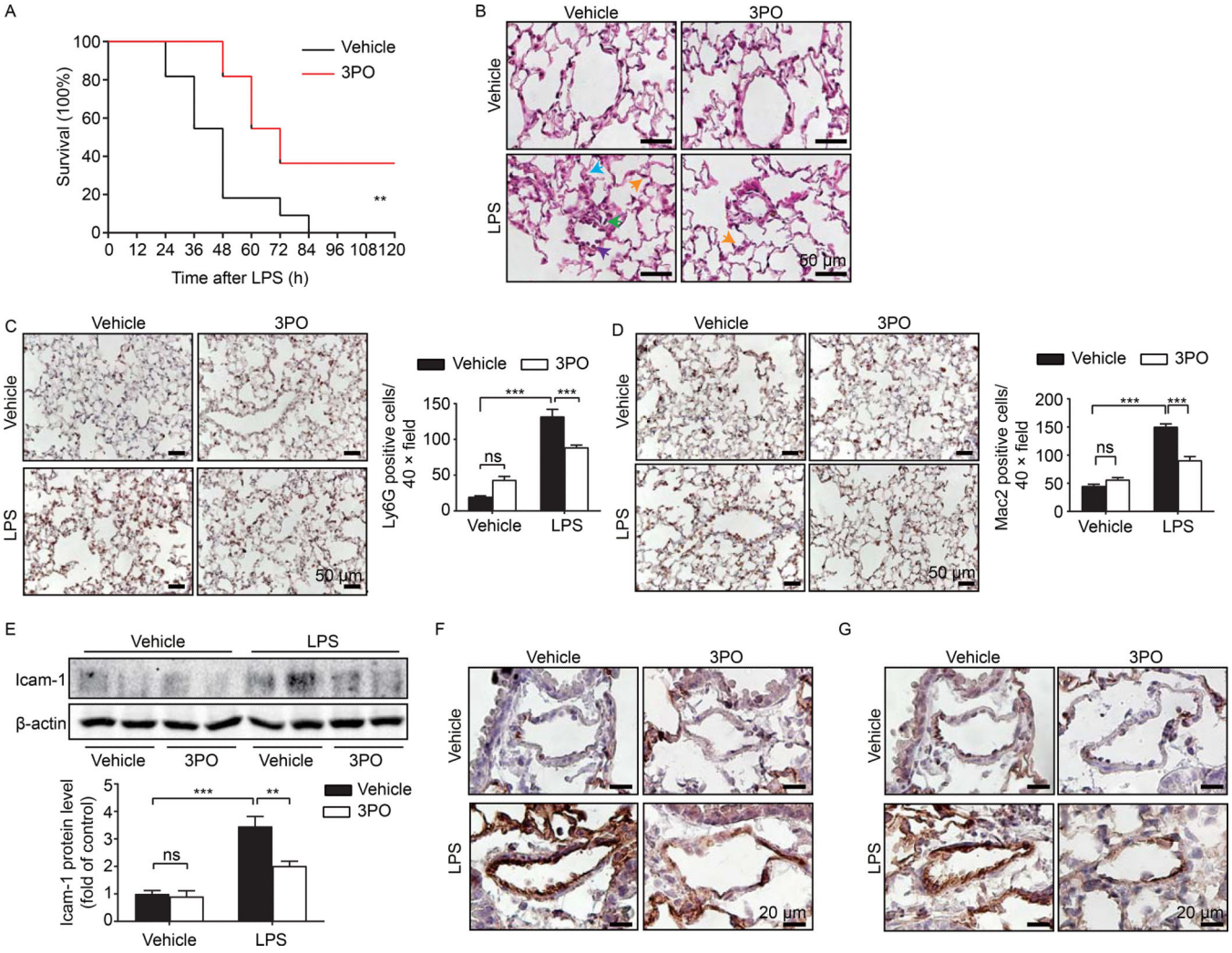

Fig. 8. 3PO treatment protects mice from LPS-induced sepsis.

(**A**) Mortality of C57 mice treated with DMSO (control) or 3PO for 3 hours followed by i.p. injection of LPS at a dose of 12.5 mg/kg body weight. Mice were monitored for 10 d. n = 10 mice per group. Statistical analysis was performed using log-rank test, ** $p < 0.01$. (**B**) Representative images of hematoxylin and eosin staining of lung sections from control mice and 3PO pre-treated mice exposed to vehicle or 12.5 mg/kg LPS for 6 hours. Scale bars, 50 μm. Green arrows indicate neutrophils in the alveolar space, yellow arrows indicate neutrophils in the interstitial space, purple arrows indicates macrophages, and blue arrows indicate thickening of the alveolar walls. (**C and D**) Representative images and quantification for immunohistochemical staining of Mac 2 (**C**) and Ly6G (**D**) in lung sections from DMSO or 3PO pre-treated mice injected with vehicle or 12.5 mg/kg LPS for 6 hours. Scale bar, 50 μm. n = 6. (**E**) Western blot and densitometric quantification analysis of Icam-1 protein level in lung homogenates of DMSO or 3PO pre-treated mice challenged with vehicle or 12.5 mg/kg LPS for 6 hours. n = 6. (**F and G**) Representative images for immunohistochemical staining of Icam-1 (**F**) and Vcam-1 (**G**) in lung sections from DMSO or 3PO pre-treated mice after vehicle or 12.5 mg/kg LPS challenge for 6 hours. Scale bar, 20

μm. Data are presented as means ± SEM. Statistical significance was determined by one-way ANOVA followed by Bonferroni test. ** $p < 0.01$, *** $p < 0.001$.

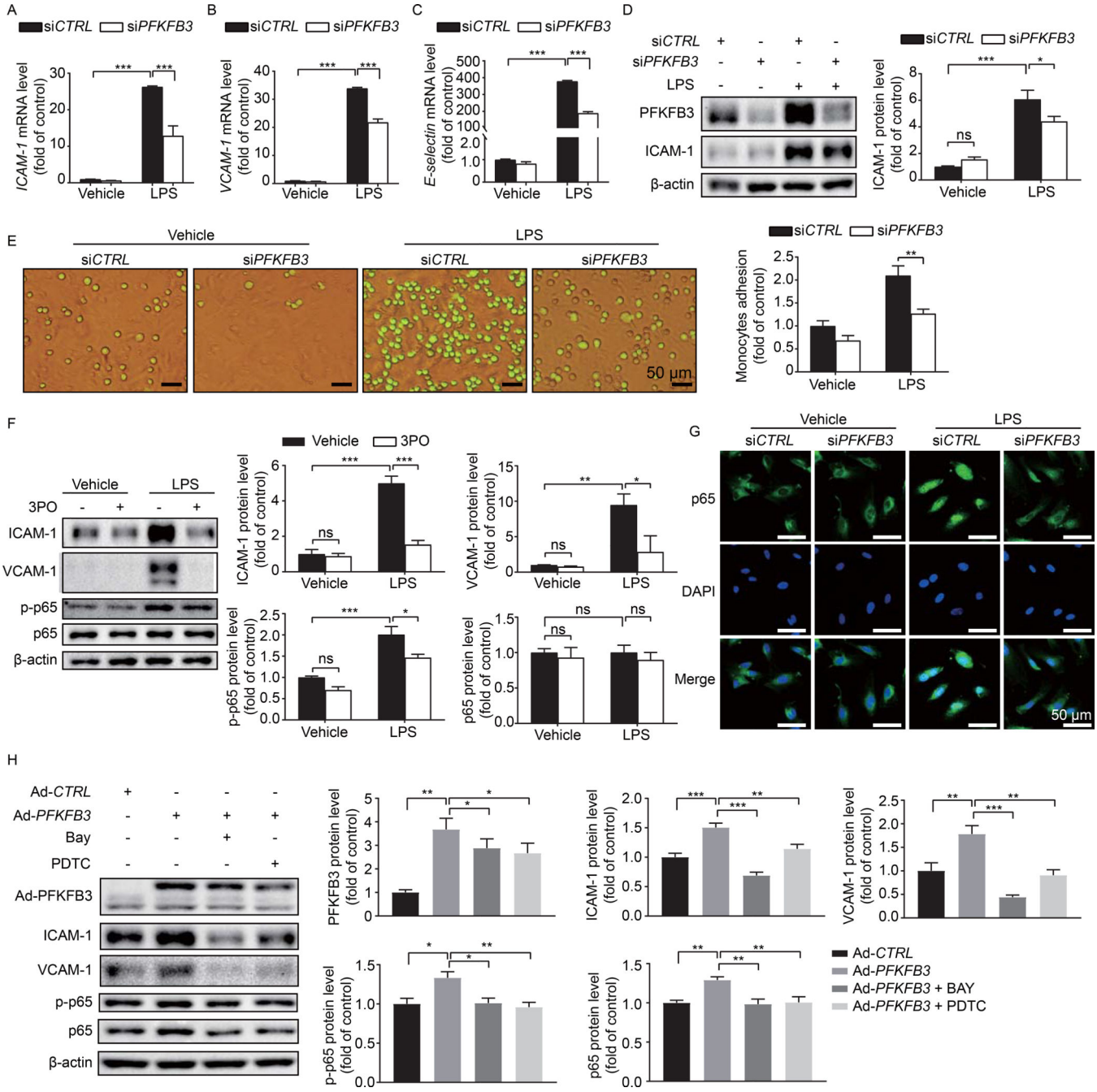

Fig. 9. *PFKFB3* knockdown decreases adhesion molecule expression via NF-κB pathway in HPAECs.

(**A-C**) Real time-PCR analysis of *ICAM-1* (**A**), *VCAM-1* (**B**), and *E-selectin* (**C**) mRNA levels in HPAECs treated with 1 μg/mL LPS for 4 h following transfection with si*CTRL* or si*PFKFB3* for 48 hours. n = 6. (**D**) Western blot analysis of PFKFB3 and ICAM-1 protein expression and densitometric quantification of ICAM-1 in HPAECs. HPAECs were transfected with si*CTRL* or si*PFKFB3* for 48 hours followed by 1 μg/ml LPS treatment for 4 hours. n = 5. (**E**) Representative images and quantification of monocyte adhesion to HPAECs transfected with si*CTRL* or si*PFKFB3* and treated with 1 μg/mL LPS for 4 h. n =

3. (**F**) Western blot analysis and densitometric quantification of ICAM-1, VCAM-1, p65, and p-p65 protein expression in HPAECs treated with LPS. HPAECs were pretreated with 20 μM 3PO for 30 min, and then treated with 1 μg/mL LPS for 4 h. n = 5. (**G**) Representative images of p65 immunostaining in HPAECs transfected with si*CTRL* or si*PFKFB3* followed by 1 μg/mL LPS treatment for 4 hours. (**H**) Western blot analysis and densitometric quantification of PFKFB3, ICAM-1, VCAM-1, p65, and p-p65 protein expression in HPAECs after PFKFB3 overexpression with or without p65 inhibitor, Bay or PDTC, treatment. n = 5. Data are represented as means ± SEM. Statistical significance was determined by one-way ANOVA followed by Bonferroni test. *$p < 0.05$ was considered significant, ** $p < 0.01$, *** $p < 0.001$.

Table 1.

Reaction system for F-2,6-P2 level assay.

Substrate	Initial concentration	Final concentration
Tris-HCl (pH7.5)	50 mM	50 mM
NADH	20 mM	0.2 mM
DTT	1 M	5 mM
F6P	200 mM	1 mM
MgCl2	1 M	2 mM
Aldolase	700 U/mL	0.7 U/mL
GDH	450 U/mL	0.45 U/mL
TIM	1200 U/mL	0.6 U/mL
PPi-PFK	C	10 μg

Table 2.

Sequences of forward and reverse primers used in Real-Time PCR analysis.

Gene name	Forward primer (5'-3')	Reverse primer (5'-3')
Murine/Human *18s* rRNA	CTTAGAGGGACAAGTGGCG	ACGCTGAGCCAGTCAGTGTA
Murine *pfkfb3*	GATCTGGGTGCCCGTCGATCACCG	CAGTTGAGGTAGCGAGTCAGCTTC
Murine *Icam-1*	GTGGCGGGAAAGTTCCTG	CGTCTTGCAGGTCATCTTAGGAG
Murine *Vcam-1*	AGTTGGGGATTCGGTTGTTC	CATTCCTTACCACCCCATTG
Murine *Il-1β*	TGTCTTGGCCGAGGACTAAGG	TGGGCTGGACTGTTTCTAATGC
Murine *Tnf-α*	AGGGTCTGGGCCATAGAACT	CCACCACGCTCTTCTGTCTAC
Murine *Cxcl10*	GAGCCTATCCTGCCCACG	GGAGCCCTTTTAGACCTT
Murine *Mcp1*	TTAAAAACCTGGATCGGAACCAA	GCATTAGCTTCAGATTTACGGGT
Human *ICAM-1*	GGCCGGCCAGCTTATACAC	TAGACACTTGAGCTCGGGCA
Human *VCAM-1*	TCAGATTGGAGACTCAGTCATGT	ACTCCTCACCTTCCCGCTC
Human *E-selectin*	CCCGAAGGGTTTGGTGAG	TAAAGCCCTCATTGCATTGA